JGR Planets

RESEARCH ARTICLE
10.1029/2019JE006307

Special Section:
Investigations of Vera Rubin Ridge, Gale Crater

A Lacustrine Paleoenvironment Recorded at Vera Rubin Ridge, Gale Crater: Overview of the Sedimentology and Stratigraphy Observed by the Mars Science Laboratory Curiosity Rover

L. A. Edgar[1], C. M. Fedo[2], S. Gupta[3], S. G. Banham[3], A. A. Fraeman[4], J. P. Grotzinger[5], K. M. Stack[4], N. T. Stein[5], K. A. Bennett[1], F. Rivera-Hernández[6], V.Z. Sun[4], K. S. Edgett[7], D. M. Rubin[8], C. House[9], and J. Van Beek[4]

[1]USGS Astrogeology Science Center, Flagstaff, AZ, USA, [2]Department of Earth and Planetary Sciences, University of Tennessee, Knoxville, TN, USA, [3]Department of Earth Science & Engineering, Imperial College London, London, UK, [4]Jet Propulsion Laboratory, California Institute of Technology, Pasadena, CA, USA, [5]Division of Geological and Planetary Sciences, California Institute of Technology, Pasadena, CA, USA, [6]Department of Earth Science, Dartmouth College, Hanover, NH, USA, [7]Malin Space Science Systems, San Diego, CA, USA, [8]Department of Earth and Planetary Sciences, University of California, Santa Cruz, CA, USA, [9]Departmen of Geosciences, Pennsylvania State University, State College, PA, USA

Key Points:
- Six sedimentary facies were identified at and just below Vera Rubin ridge and comprise three members of the Murray formation
- Vera Rubin ridge records deposition in a lacustrine environment, which expands the duration of habitable conditions observed in Gale
- The facies and stratigraphy identified here serve as a framework for interpreting strata within the Glen Torridon region and beyond

Correspondence to:
L. A. Edgar,
ledgar@usgs.gov

Citation:
Edgar, L. A., Fedo, C. M., Gupta, S., Banham, S. G., Fraeman, A. A., Grotzinger, J. P., et al. (2020). A lacustrine paleoenvironment recorded at Vera Rubin ridge, Gale crater: Overview of the sedimentology and stratigraphy observed by the Mars Science Laboratory Curiosity rover. *Journal of Geophysical Research: Planets*, *125*, e2019JE006307. https://doi.org/10.1029/2019JE006307

Received 5 DEC 2019
Accepted 24 FEB 2020
Accepted article online 10 MAR 2020

Abstract For ~500 Martian solar days (sols), the Mars Science Laboratory team explored Vera Rubin ridge (VRR), a topographic feature on the northwest slope of Aeolis Mons. Here we review the sedimentary facies and stratigraphy observed during sols 1,800–2,300, covering more than 100 m of stratigraphic thickness. Curiosity's traverse includes two transects across the ridge, which enables investigation of lateral variability over a distance of ~300 m. Three informally named stratigraphic members of the Murray formation are described: Blunts Point, Pettegrove Point, and Jura, with the latter two exposed on VRR. The Blunts Point member, exposed just below the ridge, is characterized by a recessive, fine-grained facies that exhibits extensive planar lamination and is crosscut by abundant curvi-planar veins. The Pettegrove Point member is more resistant, fine-grained, thinly planar laminated, and contains a higher abundance of diagenetic concretions. Conformable above the Pettegrove Point member is the Jura member, which is also fine-grained and parallel stratified, but is marked by a distinct step in topography, which coincides with localized meter-scale inclined strata, a thinly and thickly laminated facies, and occasional crystal molds. All members record low-energy lacustrine deposition, consistent with prior observations of the Murray formation. Uncommon outcrops of low-angle stratification suggest possible subaqueous currents, and steeply inclined beds may be the result of slumping. Collectively, the rocks exposed at VRR provide additional evidence for a long-lived lacustrine environment (in excess of 10^6 years via comparison to terrestrial records of sedimentation), which extends our understanding of the duration of habitable conditions in Gale crater.

Plain language summary The primary goal of the Mars Science Laboratory Curiosity rover mission is to explore and assess ancient habitable environments on Mars. This requires a detailed understanding of the environments recorded by sedimentary rocks exposed at the present-day surface in Gale crater. Here we review the types of sedimentary rocks exposed at a location known as Vera Rubin ridge. We find that the rocks at Vera Rubin ridge record an ancient lake environment and are a continuation of underlying lake deposits. Ancient lake deposits are highly desirable targets in the search for habitable environments, due to their ability to concentrate and preserve organic matter. This study significantly expands the duration of habitable conditions that can be confirmed through ground truth of sedimentary rocks and provides a framework for interpreting strata that lie ahead as Curiosity continues to explore Aeolis Mons.

1. Introduction

The primary goal of the Mars Science Laboratory (MSL) Curiosity rover mission is to explore, reconstruct, and assess ancient habitable environments on Mars (Grotzinger et al., 2012). To do so requires a detailed understanding of the depositional environments recorded in sedimentary rocks exposed at the surface in

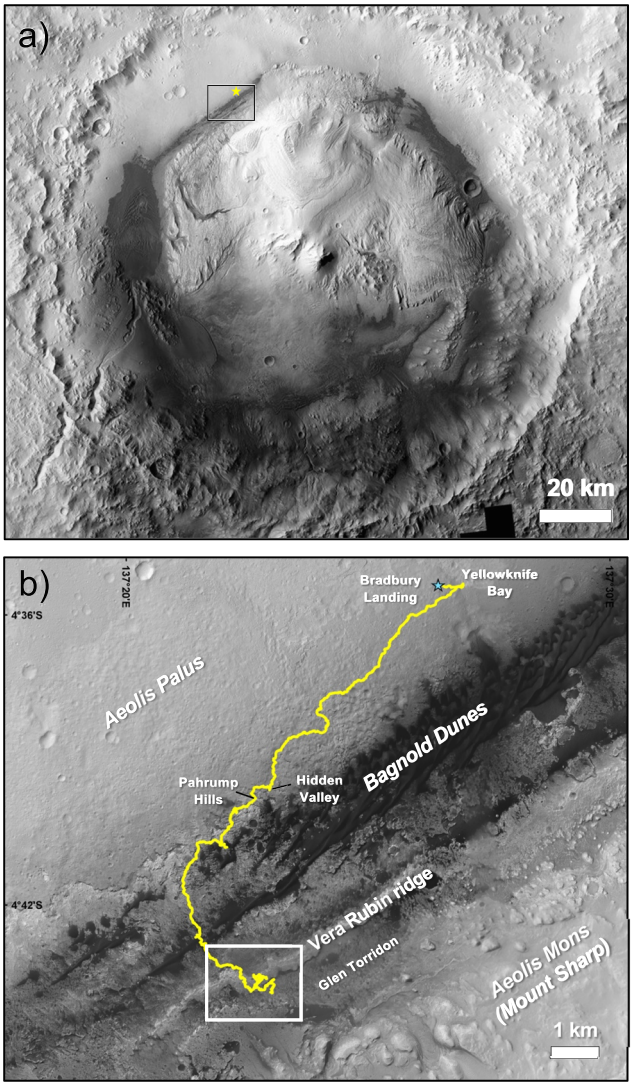

Figure 1. (a) Mars Reconnaissance Orbiter Context Camera (CTX) mosaic of Gale crater. The yellow star indicates the Mars Science Laboratory (MSL) landing site at Bradbury Landing. The black box indicates the location of (B). (b) MSL traverse path from landing through the rover's exploration of Vera Rubin ridge represented by yellow line. The white box shows the location of this study and area of Figure 3.

Gale crater, including characterization of the role and duration of ancient aqueous environments. Since landing in Gale (Figure 1), the Curiosity rover team has been able to investigate a diverse array of siliciclastic sedimentary rocks, interpreted to have formed in fluvial, deltaic, lacustrine, and eolian environments (Banham et al., 2018; Edgar et al., 2017; Grotzinger et al., 2014; Grotzinger et al., 2015; Rice et al., 2017; Stack et al., 2019; Williams et al., 2013). Ancient lacustrine deposits are highly desirable targets in the search for habitable environments, due to their ability to concentrate and preserve organic matter (Farmer & DesMarais, 1999; Hays et al., 2017; Meyers & Ishiwatari, 1995; Summons et al., 2011).

Gale crater was selected as the MSL landing site, in part because observations based on data from orbiting instrumentation revealed key environmental transitions recorded as mineralogic variability in time-ordered strata exposed on the northwest slope of Aeolis Mons (informally known as Mount Sharp; Grotzinger et al., 2012; Golombek et al., 2012). Mount Sharp, the central mound within Gale crater, is a 5-km-thick succession of intact stratigraphy, the textural and mineralogical properties of which are inferred to record changes in aqueous and climate conditions during a key transition in the history of Mars (Milliken et al., 2010). One of the unique features identified in images acquired from orbit within the stratigraphic succession that makes up Mount Sharp is a distinct geomorphic unit named the Vera Rubin ridge (VRR). Prior to landing in Gale crater, VRR was identified as a target of interest due to its associated hematite signature in orbiter-based spectroscopic data (Fraeman et al., 2013; Fraeman et al., 2016), with the potential that this hematite signals the presence of abundant liquid water at some time during the depositional or diagenetic history of the rocks exposed on the ridge. The aim of the MSL campaign at VRR was to investigate the sedimentary lithologies and facies comprising VRR bedrock strata and determine their geochemistry and mineralogy. The Curiosity rover spent nearly 500 Martian solar days (sols; 500 Mars days; 1.4 Earth years) investigating VRR rocks.

The objectives of this paper are to (i) characterize the stratigraphy of VRR strata in relation to strata of the Mount Sharp group, (ii) describe sedimentary facies and interpret them in terms of depositional processes, (iii) characterize lateral variations in facies within the ridge, (iv) reconstruct the paleoenvironmental setting of VRR strata, and (v) discuss implications for Martian climate and habitability.

2. Geologic Setting

Gale crater is an ~155-km diameter impact crater located at 5.3°S, 222.3°W, on the topographic boundary that separates the heavily cratered southern highlands from the relatively smooth northern lowlands of Mars. Crater counts suggest that Gale crater formed at approximately ~3.7 ± 0.1 Ga (Le Deit et al., 2012; Thomson et al., 2011), around the time that the planet transitioned from the Noachian to the Hesperian period.

Since landing in August of 2012, Curiosity's traverse path (Figure 1b) has been determined by the science team using a combination of interpretations based on data acquired from orbit and by data acquired on the ground via the rover. In the search for records of ancient habitable environments, Curiosity has traversed more than 20 km and gained more than 370 m in elevation.

Early in the mission (~sols 121–308), the Curiosity rover team investigated a 1.5-m-thick interval of clay-bearing mudstones in the Yellowknife Bay formation, interpreted as a record of the first habitable environment explored by the rover (Grotzinger et al., 2014). The Sheepbed member of the Yellowknife Bay formation was described as fine-grained (grain sizes < 50 μm), uniform, and laterally extensive, and was inferred to

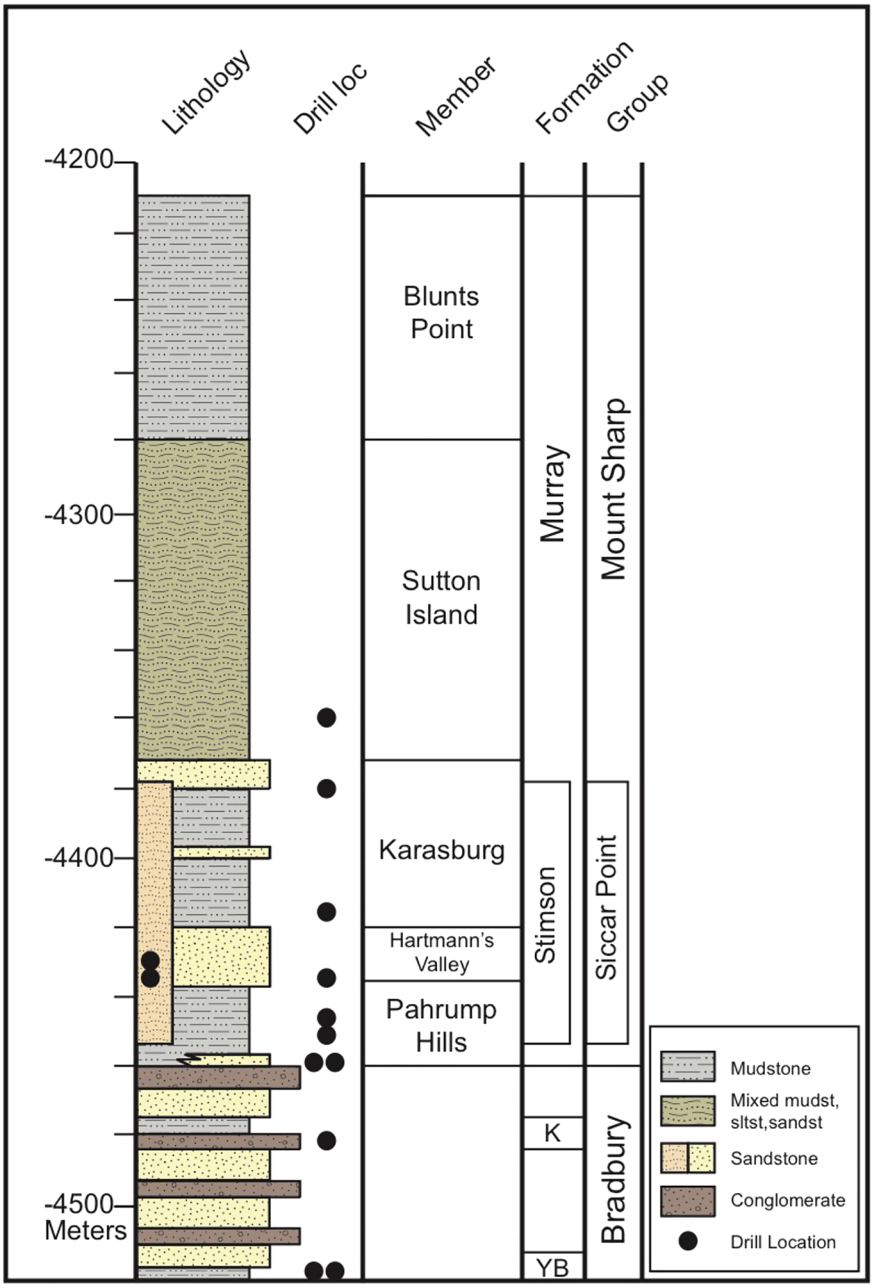

Figure 2. Generalized stratigraphic column prior to arrival at Vera Rubin ridge (sols 0–1,800). "YB" represents the Yellowknife Bay formation, and "K" represents the Kimberley formation. Column illustrates the progression from fluvial and deltaic conglomerates and sandstones in the Bradbury group to finer-grained lacustrine facies in the Murray formation. The Stimson formation unconformable overlies the Murray formation and is depicted over the elevation range in which it was encountered.

have formed via settling from suspension in a lacustrine environment. Analyses of the geochemistry and mineralogy of the mudstone indicate that the environment had a neutral pH, low salinity, all of the necessary biogenic elements, and variable redox states (Grotzinger et al., 2014). However, as the Sheepbed member was the stratigraphically lowest member within the Yellowknife Bay formation, its thickness, and hence the inferred duration of habitable conditions, was limited in scope.

Subsequently, the rover drove southward and upward toward the lower reaches of Mount Sharp, across fluvial (Edgar et al., 2018; Williams et al., 2013) and deltaic (Grotzinger et al., 2015) facies. The facies associations and observed southward transport direction predicted that the rover would eventually encounter

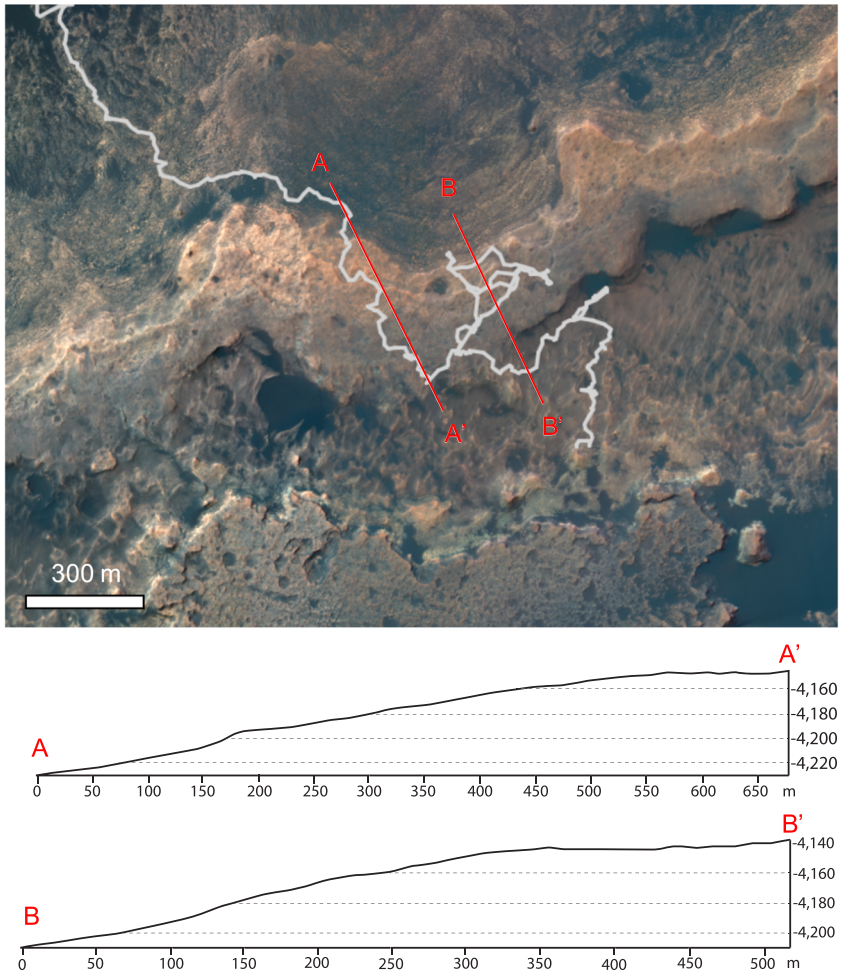

Figure 3. Curiosity's traverse path across Vera Rubin ridge. Exploration initially progressed from northwest to southeast, then northeast to investigate an area with a high hematite signature (Fraeman et al., 2018). The unique traverse path enabled two distinct transects through the stratigraphy. The gray line shows the traverse path from sols 1,664 to 2,582. The red lines correspond to approximate eastern and western transects and correspond to profiles shown below.

deposits from a body of standing water. This was confirmed when the rover drove into Hidden Valley and the Pahrump Hills and the team discovered a thick succession of fine-grained, well laminated rocks, interpreted to have formed through lacustrine deposition (Grotzinger et al., 2015; Rivera-Hernández et al., 2019; Stack et al., 2019). Evidence for plunging river plumes at the Pahrump Hills favors a freshwater lacustrine origin based on paleohydraulic modeling (Stack et al., 2019). These lacustrine mudstones were informally termed the Murray formation. With the exception of modern and ancient eolian deposits that unconformably overlie the Murray formation (Banham et al., 2018), the Curiosity rover has predominantly been driving through the Murray formation for the past 5.5 Earth years.

As the mission progressed and the rover continued to drive southward and upward, the team developed a working stratigraphic column (Figure 2). This stratigraphic column represents a sedimentary log of the lithologies that the rover encountered over a lateral distance of more than 10 km. It should be noted that the column represents both a vertical component of stratigraphic climb assuming approximate horizontality of strata and a lateral component as the rover has driven to the south. The sedimentary succession is presented as a single column for simplicity but should not be taken as a true vertical succession at a single location.

For much of the mission, the rover has only made unidirectional progress—rarely returning to stratigraphic sections adjacent to previously explored areas—so the composite stratigraphic column does not account for

lateral facies variability. At the time of writing, the stratigraphic column records more than 370 m of elevation. The Murray formation covers more than 300 m of the 370 m of strata explored to date. Prior to arrival at VRR, five distinct stratigraphic members were recognized within the Murray formation based on subtle changes in lithology (Fedo et al., 2019), as detailed below.

The Murray formation is a succession of sedimentary rocks that consist predominantly of mudstones that are interpreted to have been deposited in a lake or marginal lake setting (e.g., Fedo et al., 2018, 2019; Grotzinger et al., 2015; Rivera-Hernández et al., 2019, 2020; Stack et al., 2019). The lowest exposed stratigraphic member of the Murray formation is the Pahrump Hills member (Figure 2), which is defined by millimeter- to centimeter-scale laminated mudstone to very fine sandstone, with decimeter- to meter-scale scour-and-drape structures. It is interpreted to record suspension fallout in a lacustrine environment with occasional event beds formed by plunging river plumes (Minitti et al., 2019; Stack et al., 2019). The Pahrump Hills member is overlain by the Hartmann's Valley member, which includes meter-scale trough cross stratification and is interpreted to be consistent with eolian or fluvial deposition in a lake margin setting (Gwizd et al., 2018, 2019). The Karasburg member of the Murray formation is composed mainly of millimeter- to centimeter-scale parallel laminated mudstone that preserves abundant phyllosilicate minerals (Rampe et al., 2017), with two distinct interbeds of cross-bedded sandstone. The Karasburg member is interpreted to have formed principally in a low-energy lacustrine environment with stable water levels, as evidenced by the lack of disruption of laminae indicating a lack of desiccation, and absence of higher energy, lake-margin, eolian, or fluvial sandstone. Stratigraphically above the Karasburg member lies the heterolithic Sutton Island member, which is recognized as a finely laminated mudstone to siltstone with centimeter-scale ripple cross lamination to decimeter-scale cross stratification, and the presence of possible desiccation cracks (Stein et al., 2018). It is interpreted to have formed via a mixture of depositional processes in a lacustrine and lake margin setting. Prior to arrival at VRR, the rover encountered an additional member of the Murray formation, known as the Blunts Point member. The Blunts Point member is a mudstone with extensive planar lamination. Outcrops are crosscut by abundant fine fractures and curvi-planar calcium sulfate veins, which commonly obscure primary sedimentary structures (Fedo et al., 2018, 2019). The Blunts Point member indicates that the Sutton Island member did not represent the final drying out of the lake, but instead, the environment shifted back into a stable lacustrine setting (Rivera-Hernández et al., 2020). The analysis of these members provides important context for exploration of the VRR strata and raise questions about the duration of habitable conditions recorded in the rocks of lower Aeolis Mons in Gale crater, and the variation in chemistry of these strata. In this paper we describe the Blunts Point member in more detail and characterize two additional members of the Murray formation, covering more than 100 m of stratigraphic thickness.

3. Data and Methods

3.1. The Vera Rubin Ridge Campaign

Curiosity's ground-based investigation of VRR began with a close-approach for imaging starting on sol 1,726, and subsequent ascent starting around sol 1,800. Several key regions on the ridge were identified based on examination of Mars Reconnaissance Orbiter (MRO) High Resolution Imaging Science Experiment (HiRISE) images as waypoints for more in-depth rover-based investigations. The initial traverse was planned to progress from north to south across the ridge and to sample areas that were identified as having distinct textural and spectral properties based on orbiter data. During this time, the MSL Team worked to develop a new method to drill, after having been suspended following the “Sebina” drill campaign (sol 1,495). When the drill became available for sample extraction again (sol 1,977), the team decided to descend VRR and drive north to sample the Blunts Point member so that every member of the Murray formation would be sampled. Efforts to drill both strata that comprise VRR and the Blunts Point member resulted in an extensive traverse path that enabled two distinct, approximately north-south, transects across the ridge (Figure 3); this allowed correlation of sedimentary facies across a lateral distance of several hundred meters. Stratigraphic correlation of this extent had not been possible previously during the mission. Ultimately, the VRR campaign resulted in 500 sols of science analyses, including four drill samples (13 previous drill samples are depicted on Figure 2). Complete details of the VRR campaign are described by Fraeman et al. (2018).

Table 1
Targets for Assessment of Laminae Thickness

Target	Sol	Elevation (m)	Average thickness (mm)	Member
Hexriver	1,879	−4,167	0.38	Jura
Klipfonteinheuwel	1,886	−4,167	0.32	Jura
Drakensberg	1,892	−4,158	0.3	Jura
Strubenkop	1,892	−4,158	0.29	Jura
Muck	1,897	−4,157	0.29	Jura
Wick	1,897	−4,157	0.27	Jura
Haroldswick	1,922	−4,154.5	0.37	Jura
Crinan	1,925	−4,153.5	0.38	Jura
Canna	1,932	−4,149	0.25	Jura
Rhum	1,935	−4,149	0.3	Jura
Knoydart	1,940	−4,148.5	0.22	Jura
Mallaig	1,940	−4,148.5	0.25	Jura
Barkeval	1,988	−4,151	0.41	Jura
North_Harris	1,988	−4,151	0.38	Jura
Dun_Caan	2,008	−4,161	0.33	Pettegrove Point
Babbitt	2,029	−4,166	0.38	Pettegrove Point
Nashwauk	2,038	−4,181.5	0.44	Pettegrove Point
Bald_Eagle_Lake	2,042	−4,179	0.34	Pettegrove Point
Sasanoa	1,811	−4,200	0.57	Pettegrove Point
Mount_Ephraim	1,811	−4,200	0.27	Pettegrove Point
N181611[a]	1,816	−4,196.5	0.38	Pettegrove Point
N181609[a]	1,816	−4,196.5	0.42	Pettegrove Point
Christmas_Cove	1,818	−4,196.5	0.59	Pettegrove Point
Whittum	1,818	−4,196.5	0.4	Pettegrove Point
Duluth	2,055	−4,192.5	0.3	Blunts Point

Abbreviation: MAHLI: Mars Hand Lens Imager.
[a]Targets N181611 and N181609 were MAHLI targets that were imaged as candidate Dust Removal Tool (DRT) targets to assess the topography of these rocks prior to dust removal.

3.2. Instruments and Data

The stratigraphy and sedimentology (sedimentary textures, grain size, and sedimentary structures) of VRR strata were documented using the Mast Cameras (Mastcams), Navigation Cameras (Navcams), Hazard Cameras (Hazcams), Mars Descent Camera (MARDI), Mars Hand Lens Imager (MAHLI), and the Remote Micro Imager (RMI) subsystem of the Chemistry Camera (ChemCam) instrument. These instruments provide images at spatial scales ranging from several centimeters per pixel down to tens of micrometers per pixel. Details of the geochemical and mineralogic analyses are described by Thompson et al. (2019), Frydenvang et al. (2018), and Morris et al. (2019).

The Mastcam, Navcam, and ChemCam instruments are located on the rover's Remote Sensing Mast, mounted approximately 2 m above the ground. Mastcam consists of two digital cameras with focal lengths of 34 mm (M34) and 100 mm (M100), which provide pixel scales of 0.22 and 0.074 mrad/pixel, respectively. Mastcam is capable of producing full color, panoramic and stereoscopic mosaics (Malin et al., 2017) ideal for recognizing sedimentary facies, textural and spectral variability, sedimentary structures, and bedding orientations. All of these characteristics are used to make subsequent stratigraphic correlations.

The Navcam instrument consists of four digital cameras that provide panoramic and stereoscopic imaging. There are two pairs of Navcams, but only one pair is active at a time. Navcam has a 45° field of view and a pixel scale of 0.82 mrad/pixel (Maki et al., 2012). Navcam images were used to provide additional geologic context and to select targets across VRR.

The ChemCam instrument consists of a laser-induced breakdown spectrometer (LIBS) and remote microimager (RMI), which are used to provide remote elemental compositions at distances up to ~7 m from the mast and to provide high-resolution gray-scale documentation images (Maurice et al., 2012; Wiens et al., 2012). The RMI has a field of view of 20 mrad and a pixel scale of 19.6 μrad per pixel (Le Mouélic et al., 2015). In addition to providing geochemical observations, the ChemCam LIBS and RMI were used for identification of grain sizes (Rivera-Hernández et al., 2019); RMI data also contribute to investigation of sedimentary structures.

MAHLI is a high spatial resolution camera located at the end of the rover's robotic arm. MAHLI provides color and stereoscopic imaging and operates at working distances between 2.1 cm to infinity. MAHLI is capable of acquiring images with a maximum high resolution of ~14 μm per pixel (Edgett et al., 2012), which enables the distinction of silt-sized grains from very fine sand. The highest spatial resolution images acquired under typical usage conditions are in the 16 to 32 μm per pixel range (Yingst et al., 2016). MAHLI images were used to study grain size, stratification, and small-scale sedimentary structures across VRR (Bennett et al., 2018).

MARDI is a fixed focal length nadir-pointed camera located underneath the front port side of the rover (Malin et al., 2017). The camera was initially intended to localize the landing site within Gale crater during descent but has since been used to document the terrain beneath the rover (Minitti et al., 2019). MARDI has a field of view of ~70° by 52° and provides in-focus images from working distances of 2 m to infinity.

MARDI images were used to document changes in bedrock beneath the rover and to provide additional geologic context.

The Curiosity rover also contains four pairs of Engineering Hazard Assessment Cameras (Hazcams) mounted on the lower portion of the front and rear of the rover (Maki et al., 2012). Each camera has a 120° field of view and a pixel scale of 2.1 mrad/pixel. Hazcam images were used to map out terrain, select targets, and provide additional geologic context.

3.3. Determination of Laminae Thickness

The thickness of lamination was characterized based on visual inspection of MAHLI images. Laminae thicknesses were calculated based on the pixel separation between the center of laminae identified along digitized transects drawn orthogonally through mapped laminae. Lamination thicknesses were measured orthogonally to the bedding to account for the varying orientation of the exposed rocks. The pixel resolution of each MAHLI image was approximated from the standoff distance of the MAHLI instrument. Measurements of surfaces especially oblique relative to bedding were either discarded or corrected for their orientation if there was sufficient corresponding stereo information from Mastcam images. The arithmetic mean and one standard deviation in lamination thickness were computed for each target. Twenty-five targets were selected for evaluation of laminae thickness (Table 1 and also, see data repository), focused on targets with appropriate relief and sufficient stereo coverage.

3.4. Determination of Grain Size

Grain sizes were determined via visual inspection of MAHLI images, supplemented using ChemCam LIBS and the Gini Index Mean Score (GIMS) to infer grain size. MAHLI acquired images at a total of 146 distinct rock targets across VRR, with standoff distances ranging from ~1 to ~25 cm, yielding pixel scales of ~17 to ~100 μm (Bennett et al., 2018). MAHLI images were analyzed to determine grain size, stratification, and the presence or absence of small-scale diagenetic features.

Grain size was also estimated using GIMS, a grain size proxy that uses point-to-point chemical variabilities in ChemCam LIBS data (Rivera-Hernández et al., 2019). ChemCam LIBS is a destructive analysis, leaving behind small 0.4- to 0.6-mm pits that represent the points that were vaporized by the ChemCam laser (Maurice et al., 2012; Wiens et al., 2012). The diameters of these points correspond to the size of medium to coarse sand. Chemically homogeneous rocks with grains considerably smaller than the laser spot size tend toward low point-to-point chemical variability, while rocks with grains about the size of the spot or larger result in higher point-to-point chemical variability when individual grains of different composition contribute to the spectra (e.g., Rivera-Hernández et al., 2019). In this way, the presence of mud-sized grains can be inferred via low point-to-point variability, while the presence of sand-sized grains can be inferred from nonuniform compositions. Following the methods of Rivera-Hernández et al. (2019), and grain size calibration of Rivera-Hernández et al. (2020), GIMS grain size estimates were determined for 161 VRR rocks. MAHLI and ChemCam RMI images were used to exclude LIBS shots on or near diagenetic features, loose sediment, and fractures/cracks from the GIMS analysis.

4. Sedimentary Facies

Six distinct sedimentary facies were identified at VRR based on grain size, texture, and sedimentary structures (Table 2 and Figure 4). Erosional resistance was also used as a proxy for changes in grain size, cementation, and porosity, highlighting minor differences in sedimentary facies. Facies are presented in order of increasing grain size and inferred energy of deposition.

4.1. Facies 1: Recessive Weathering Evenly Planar Laminated Mudstone With Abundant Fractures and Veins

4.1.1. Description

This facies exhibits extensive planar lamination and is inferred to consist predominantly of mudstone (Figure 4a). Average laminae thicknesses are 0.3 mm. This facies is commonly crosscut by abundant fractures and millimeter-thick calcium sulfate veins. The veins are more resistant to erosion than the mudstone and crosscut at a variety of angles, from bedding parallel to high angle, which in some places obscures the primary stratification. However, the veins can be distinguished from the recessive mudstone by the appearance of thin white lineations (Figure 4b), which represent freshly exposed parts of the calcium sulfate veins

Table 2
VRR Sedimentary Facies

Facies	Description	Interpretation
1	Recessive weathering, evenly planar laminated mudstone facies with abundant fractures and veins	Fallout from suspension in a lacustrine setting
2	Resistant, evenly laminated mudstone to fine sandstone facies	Lacustrine sedimentation in a nearshore environment
3	Fine-grained thinly parallel-stratified red and gray mudstone to very fine sandstone facies with rare crystal molds	Lacustrine sedimentation in a nearshore environment with variable diagenesis
4	Alternating thinly and thickly laminated mudstone facies	Variable deposition in a lacustrine environment due to changes in sediment supply
5	Decimeter-scale cross-stratified facies	Subaqueous transport in a nearshore environment
6	Meter-scale inclined bedding	Small slope failures resulting in slumping

in contrast to the red to brown bedrock. In places that are free of veins and fractures, fine parallel laminations can be traced laterally for several meters with no disruption. This facies was observed on the traverse leading up to VRR and is exposed just below the topographic ridge (Table 2).

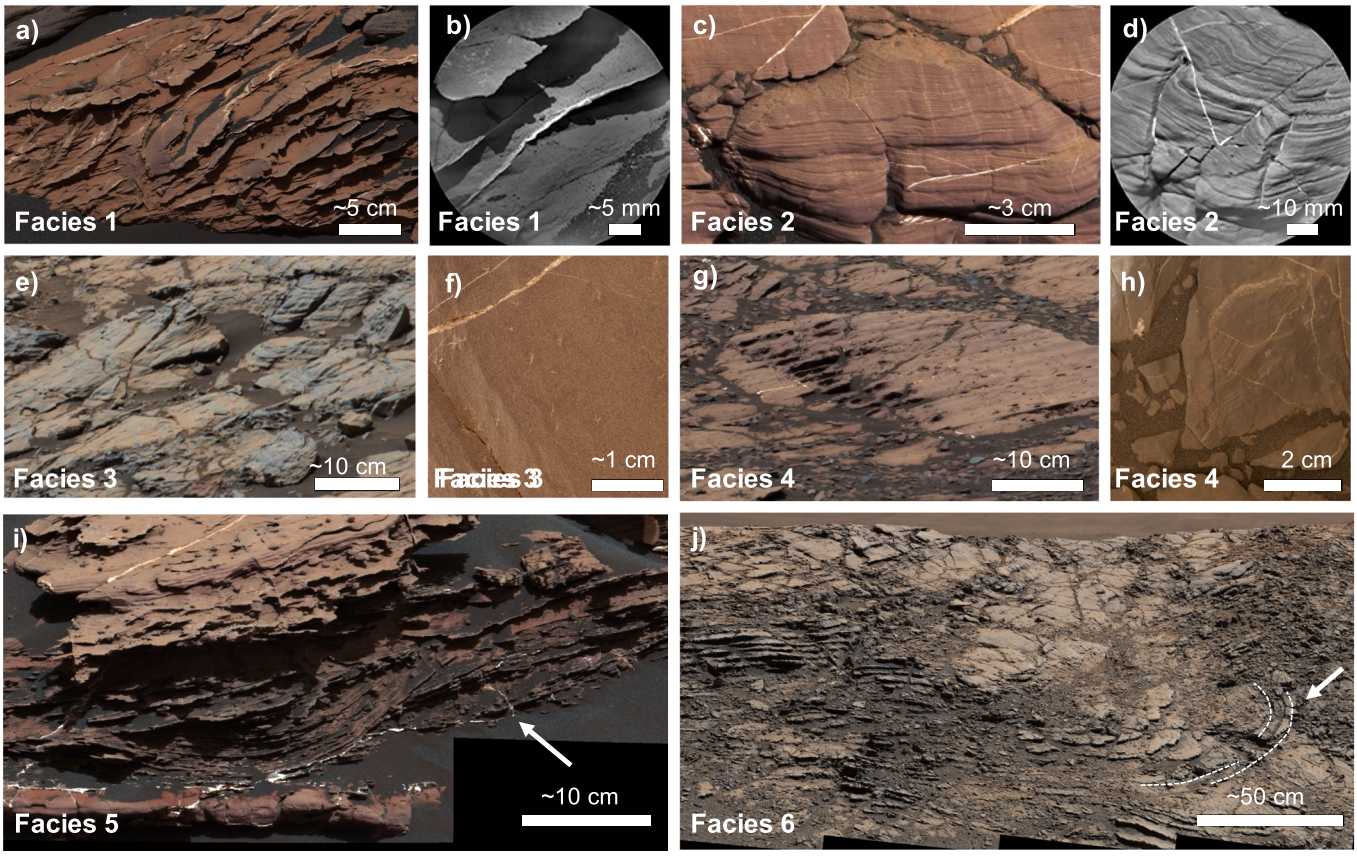

Figure 4. Sedimentary facies observed at Vera Rubin ridge. See text for full descriptions. (a) Facies 1: Recessive weathering evenly laminated mudstone with abundant fractures and veins. Mastcam M100 image acquired on sol 1,737, sequence mcam09078. (b) Facies 1 seen in ChemCam RMI acquired on sol 1,737, CR0_551693659, ChemCam sequence ccam04736. (c) Facies 2: Resistant, evenly laminated mudstone to fine-sandstone. Mastcam M100 image acquired on sol 1,812, sequence mcam09355. (d) Facies 2 observed in ChemCam RMI of target "Mount Coe" acquired on sol 1,812, CR0_558351395, ChemCam sequence ccam04811. (e) Facies 3: Fine-grained thinly parallel-stratified red and gray mudstone to very fine sandstone with occasional crystal molds. Mastcam M100 image acquired on sol 2,009, mcam10584. (f) Crystal molds in Facies 3 observed in Mars Hand Lens Imager (MAHLI) target "Seaforth Head" acquired on sol 1,991 from 5-cm standoff. MAHLI image 1991MH0002650000800144R00. (g) Facies 4: Thinly and thickly laminated mudstone facies (Flodigarry facies). Mastcam M100 image acquired on sol 2,013, sequence mcam10610. (h) Facies 4 observed in MAHLI target "Trollochy" acquired on sol 2,166. MAHLI image 2166MH0001800010802797C00. (i) Facies 5: Decimeter-scale cross-stratified facies. Mastcam M100 image acquired on sol 1,802, sequence mcam09300. (J) Facies 6: Large-scale inclined bedding. The white dashed lines trace beds that are steeper than the angle of repose, indicated by the arrow. Mastcam M100 image acquired on sol 1,946, sequence mcam10168.

4.1.2. Interpretation

This facies is interpreted to have formed through fallout of clay and/or silt-sized sediment from suspension in a lacustrine setting. The fine-grained nature, recessive weathering character, and lack of disruption of primary laminae suggest that the deposits were not subaerially exposed during deposition.

4.2. Facies 2: Resistant, Evenly Laminated Mudstone to Fine-Sandstone

4.2.1. Description

This facies is characterized as a parallel-laminated mudstone to fine sandstone that is more erosion-resistant compared to Facies 1 (Figures 4c and 4d). Laminae thicknesses range from 0.32 to 0.51 mm, with an average of 0.41 mm. Facies 2 contains fewer fractures and veins than Facies 1, though veins are still present. However, Facies 2 is more competent, and veins do not stand out in positive relief as they do in Facies 1. Facies 2 also contains a higher abundance of diagenetic nodules. GIMS analyses of Facies 2 suggest grain sizes that are mostly consistent with mudstone but also contain silt and very fine sand.

4.2.2. Interpretation

The sedimentary texture and structure of this facies are consistent with lacustrine sedimentation but may indicate a more nearshore environment relative to Facies 1, as evidenced by the introduction of coarser grains. However, the consistent, even laminations and general lack of disruption suggest fallout from suspension in a relatively stable aqueous environment.

4.3. Facies 3: Fine-Grained Thinly Parallel-Stratified Red and Gray Mudstone to Very Fine Sandstone With Occasional Crystal Molds

4.3.1. Description

This facies is characterized by parallel-stratified mudstone to very fine sandstone (Figure 4e). Fine laminae of variable thickness are traceable for up to several meters laterally with minimal disruption. Laminae thicknesses range from 0.24 to 0.41 mm, with an average of 0.31 mm. GIMS analyses of Facies 3 suggest a potentially higher abundance of rocks with very fine sand than in Facies 2. This facies also differs from Facies 1 and 2 by the occurrence of crystals and crystal molds (Bennett et al., 2018), and greater variability in color, with many notable red and gray color variations across decimeter- to meter-scale outcrops. The red and gray color variations are observed to crosscut laminae. Grain size measurements indicate that there may be minor variations between the slightly finer-grained red parts of the outcrop to the slightly coarser grained gray parts (Bennett et al., 2018). MAHLI and ChemCam targets acquired from gray parts of this facies suggest the presence of grains up to very fine sand, whereas the red parts of this facies have grain sizes that are consistent with silt and finer. Crystal molds are observed to be randomly distributed and cut across bedding planes. Crystal molds are approximately 2 mm in length, and some show swallow-tail twins. Where present, crystal molds make up a few percent of the surface area (Figure 4f).

4.3.2. Interpretation

This facies is interpreted to record fallout from suspension in a lacustrine environment. The lack of disruption of laminae suggests nonemergence. Similar to Facies 2, the presence of coarser grains may indicate proximity to a nearshore environment. Crystals and crystal molds are interpreted as a signal of the presence of early diagenetic minerals (Bennett et al., 2018). The color variations are also inferred to result from diagenesis, as evidenced by the observation of red and gray color variations crosscutting primary lamination (Fraeman et al., 2018).

4.4. Facies 4: Alternating Thinly and Thickly Laminated Mudstone Facies (Informal Unit Name, "Flodigarry Facies")

4.4.1. Description

This facies is defined by alternating thinly and thickly laminated packages of mudstone to fine-sandstone (Figures 4g and 4h). Changes in laminae thickness produce alternating erosional characteristics and color differences. Thinly laminated packages are recessive, while more thickly laminated packages are resistant, which leads to red-colored resistant beds and orange (potentially more dust-covered) recessive intervals. This facies is named after the "Flodigarry" target that was encountered on sol 2,357, after the rover had descended the south side of VRR, into the Glen Torridon region. It was given a name because it is distinct and critical for understanding the linkages between the strata exposed on VRR and in Glen Torridon (Fedo et al., 2019). Where present, the Flodigarry facies is exposed in an approximately 5- to 7-m-thick interval. Grain

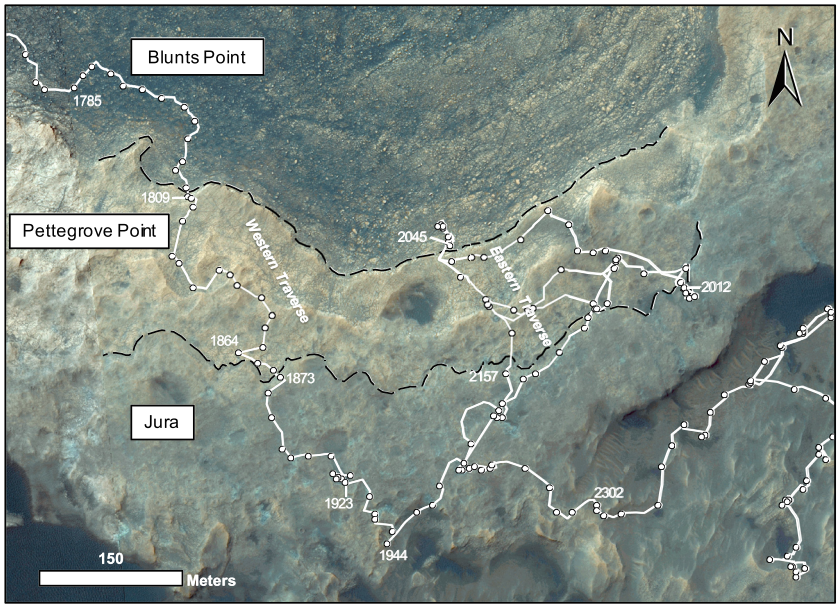

Figure 5. Vera Rubin ridge stratigraphic member boundaries shown as black dashed lines. The white line shows the traverse path from sols 1,754 to 2,481. The traverse path can be approximately divided into western and eastern sections for comparison. Numbers indicate sols for key transitions and notable outcrops.

size estimates from GIMS suggest mud to coarse silt sized grains. The average laminae thickness is approximately 0.35 mm.

4.4.2. Interpretation

This facies is interpreted to record variable deposition in a lacustrine environment. Changes in sediment supply can result in thicker less well-laminated intervals, alternating with more typical finely laminated mudstone indicative of fallout from suspension.

4.5. Facies 5: Decimeter-Scale Cross-Stratified Facies

4.5.1. Description

This facies is characterized by the appearance of decimeter-scale trough cross-bedding (Figure 4i). The facies occurs at isolated intervals and typically only represents a single bedset. Facies 5 is recognized by trough-shaped truncation surfaces that do not correspond to curvi-planar white calcium sulfate veins. MAHLI and ChemCam observations were not acquired on this facies, so grain size information is unavailable, but the grains are finer than Mastcam images can resolve. This facies typically occurs in association with Facies 2.

4.5.2. Interpretation

The presence of cross-bedding suggests deposition by subaqueous traction transport. A nearshore environment is inferred based on the association of Facies 5 with Facies 2, and the presence of cross-bedding implies sand-sized grains or silt/clay aggregates (e.g., mud pellets) was involved. Cross-bedding may record lateral migration of muddy channels or bars, migration of muddy bedforms in stratified flows (Flood & Giosan, 2002), migration of mud banks (Taylor & Purkis, 2012), or deposition by dunes made of sand-sized mud aggregates. Due to the limited observations of this facies, we are unable to distinguish between these depositional processes but recognize the influence of subaqueous currents.

4.6. Facies 6: Meter-Scale Inclined Bedding

4.6.1. Description

This facies is defined by meter-scale inclined beds and the absence of truncation surfaces (Figure 4j). Beds dip in a variety of orientations and in some places are steeper than the angle of repose. Domal, concave-down structures are observed, as are occasional verging folds (e.g., the target "Glen Tilt" observed during sols 1,942–1,946). This facies occurs near the top of the topographic ridge, at elevations ranging from −4,172 to −4,146 m. Inclined beds are traceable in packages for up to 15 m laterally and up to 2 m thick. This facies

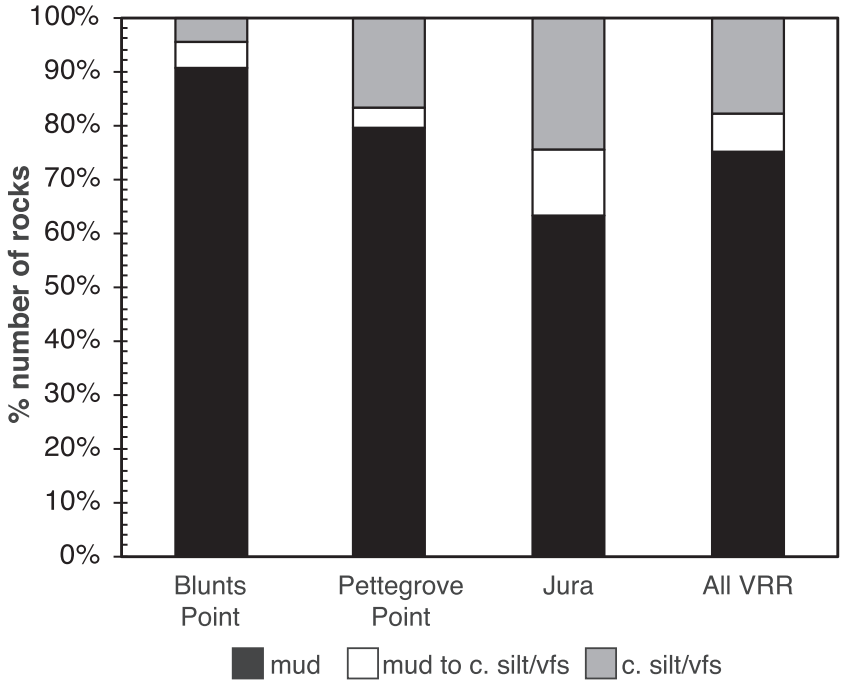

Figure 6. Grain size data estimated from Gini Index Mean Score, shown as percent abundance within each stratigraphic member, and composite through the Blunts Point, Pettegrove Point, and Jura members (far right column). A minor coarsening upward trend is observed as the percentage of rocks with very fine sand increases from the Blunts Point to Pettegrove Point to Jura members.

is often associated with Facies 3 and 4. MAHLI and ChemCam observations were not acquired on this facies, so grain size information is unavailable, but grains are finer than Mastcam images can resolve.

4.6.2. Interpretation

This facies is interpreted to record deposition from suspension in a lacustrine environment, followed by slumping due to small, localized slope failures. The lack of truncation surfaces and the presence of over-steepened beds are inconsistent with subaqueous or subaerial bedforms. The patchy lateral distribution of this facies across VRR, with the fairly constrained 26-m elevation interval in which this facies occurs, is also consistent with slumping. Beds were partially lithified prior to deformation in order to preserve these structures. Slumping may have been related to impact activity or other disturbances.

5. Stratigraphic Members

The abundance of fine-grained, parallel-stratified mudstones observed across VRR indicates that the rocks exposed on VRR are like those which occur below the ridge, between the lowermost exposed stratum of the Pahrump Hills member of the Murray formation and the uppermost stratum of the Blunts Point member of the Murray formation. In other words, the rocks exposed on VRR are also Murray formation rocks. The strata that comprise VRR are conformable with the underlying section of Murray formation rocks, with no observations that subjacent units were exposed, eroded, with their fragments incorporated into the overlying units exposed on VRR. However, a distinct topographic break occurs at the base of VRR, where the overall lithology and low-relief outcrop pattern composed of broken slabs (Blunts Point member), give way to a more distinct meters-tall cliff absent any of the low-angle Ca-sulfate veins characteristic of the Blunts Point member. Consequently, the team divided the overlying stratigraphy as the Pettegrove Point and Jura members of the Murray formation (Figure 5). Through the VRR campaign, the Curiosity team acquired remote and in situ observations of the Blunts Point, Pettegrove Point, and Jura members, with the latter two members making up the topographic feature known as VRR.

5.1. Blunts Point Member

As previously documented (Fedo et al., 2019), the Blunts Point member is defined as a fine-grained recessive facies with extensive planar lamination. GIMS analyses indicate that the Blunts Point member is

predominantly mudstone (Figure 6). While not defined by diagenetic features, this member is notably cross-cut by abundant calcium sulfate veins that stick out in positive relief compared to the more recessive background sediment. These veins show a variety of orientations, including both high-angle and bedding-parallel veins (Fedo et al., 2018). Blunts Point is dominated by Facies 1. This member was observed during sols 1,687–1,809, and again during sols 2,045–2,094 in order to acquire a drill sample at the "Duluth" target. Figure 7 shows type examples of Blunts Point member rocks at the outcrop scale to the hand lens (macrophotographic) scale.

5.2. Pettegrove Point Member

The Pettegrove Point member is distinguished from the underlying Blunts Point member by its erosional resistance, which suggests more competent bedrock due to minor changes in grain size, compaction, or cementation. It is composed of Facies 2 and 5. Although it is similar to Blunts Point in that it is fine-grained, thinly laminated, and mostly parallel-stratified, it also contains fewer veins but a higher abundance of other macroscopic diagenetic features such as nodules or concretions. These diagenetic nodules reflect changes in pathways of diagenetic fluids driven by the different character of the bedrock within this member compared to Blunts Point rocks, and the different character of the bedrock and its diagenetic setting, and might influence its geomorphic expression as observed in HiRISE data (Bennett et al., 2018). Pettegrove Point rocks are typically red in color, though minor gray patches are observed. The member was named after a prominent outcrop on the north side of VRR, imaged during Curiosity's ascent onto the ridge (Figure 8). This member was observed during sols 1,809–1,871; 1,999–2,014; 2,020–2,045; and 2,094–2,157. On sol 2,136, a sample was collected for mineral and chemical analyses at a drill hole named "Stoer."

5.3. Jura Member

The Jura member is the stratigraphically highest member of the Murray formation observed on VRR. It is easily distinguished from the underlying Pettegrove Point member in that a distinct step in topography occurs at the contact between them (Figure 5), and the Jura contains much more variability in terms of color, texture, and sedimentary structures (Figure 9). While some parts of the Jura member are expressed as erosion-resistant outcrops, other parts are more recessive and form a lag of centimeter-sized pebbles across the top of the ridge. The Jura member consists of Facies 3, 4, and 6, with Facies 4 and 6 forming the base of the section. The member was named after a location with notable red and gray color variations (Figure 9b). MAHLI images were acquired at a target named "Jura" on the gray part of the outcrop and revealed distinctive crystal pseudomorphs, and fine, continuous laminations of variable thickness (Figures 9c–9e). While the Jura member is still dominantly composed of mudstone facies, GIMS analyses suggest a higher proportion of rocks with coarser grains than the Pettegrove Point and Blunts Point members (Figure 6). The Jura member was observed during sols 1,871–1,999; 2,014–2,020; 2,157–2,302; and 2,094–2,157; drill samples "Highfield" and "Rock Hall" were collected from this unit.

6. Stratigraphic Correlation

The VRR campaign consisted of two distinct traverse paths across the ridge (Figures 3 and 5), which enabled correlation of stratigraphy across two sections, separated laterally by several hundred meters. The stratigraphic members described above were recognized by their distinct lithologic properties as expressed in Mastcam images and also correspond to clear topographic and textural changes observable in HiRISE images. As such, the contacts between these members can be mapped using orbiter (MRO HiRISE) images as informed by ground-based observations from Curiosity (Figure 5).

The same textural and lithologic transitions from Blunts Point to Pettegrove Point and from Pettegrove Point to Jura members can be observed on both the western and eastern parts of the traverse path. However, the contacts show some substantial topography from west to east (Figure 10). On the western traverse, the transition from Blunts Point to Pettegrove Point occurs at −4,209 m, whereas on the eastern traverse it occurs at −4,187 m. Similarly, the Pettegrove Point to Jura contact occurs at −4,168 m on the western traverse compared to −4,157 m on the eastern traverse. Expanding the stratigraphic member mapping beyond VRR reveals similar trends and variable topography. While the thickness of individual members is relatively consistent, the elevation at which these transitions occur is offset by approximately 10–20 m.

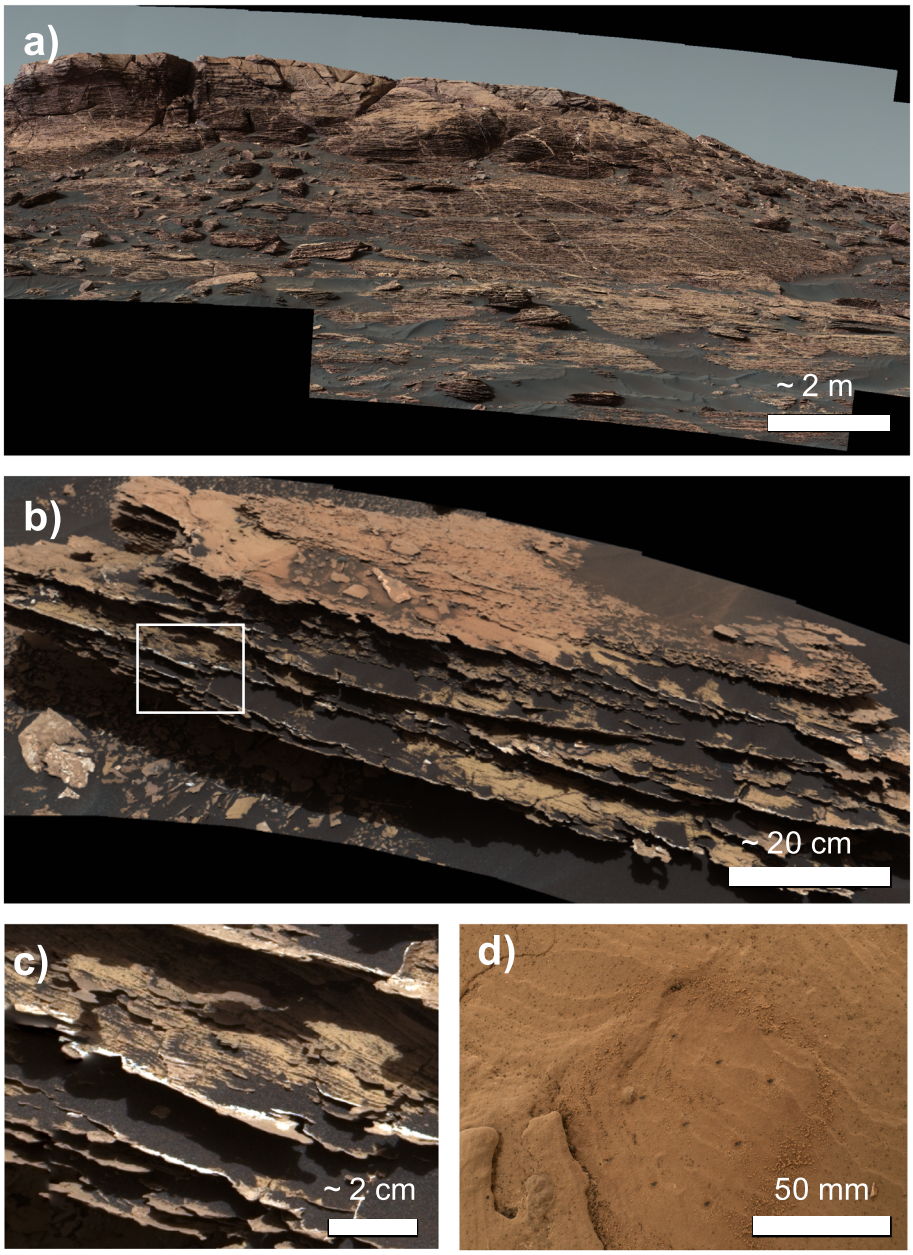

Figure 7. (a) Blunts Point member observed on the approach to Vera Rubin ridge. Horizontal laminae are crosscut by white high-angle calcium sulfate veins. This mosaic also shows the transition to the overlying Pettegrove Point member which forms the more resistant top of the outcrop. Mastcam mosaic acquired on sol 1,785 by the M100 camera, sequence mcam09211. (b) A block of the Blunts Point member showing recessive intervals interrupted by low-angle veins. The white box shows the location of (c). Mastcam image acquired on sol 1,700 by the M100 camera, sequence mcam08865. (c) Closer inspection of (b) reveals fine-grain sizes, planar lamination, and resistant bedding-parallel white veins. (d) Mars Hand Lens Imager (MAHLI) imaging confirms fine-grain sizes and thin parallel lamination. Dark spots represent a 3x3 ChemCam raster in the middle of the image. MAHLI image of target "Winter Harbor" acquired on sol 1,736 from 5-cm standoff. MAHLI image 1736MH0001220010700071C00.

This offset can be attributed to one of two explanations: VRR may have experienced differential compaction such that originally horizontal contacts are now slightly offset, or that the contacts between these members record lateral variations in facies that would naturally vary with elevation as strata accumulate due to different inputs to the sedimentary basin(s). Because this is a rare opportunity in the mission that two separate transects through the stratigraphy have been possible, it is unclear whether differential compaction occurred, though this is common in terrestrial sedimentary environments. It is thought that Gale crater may have once

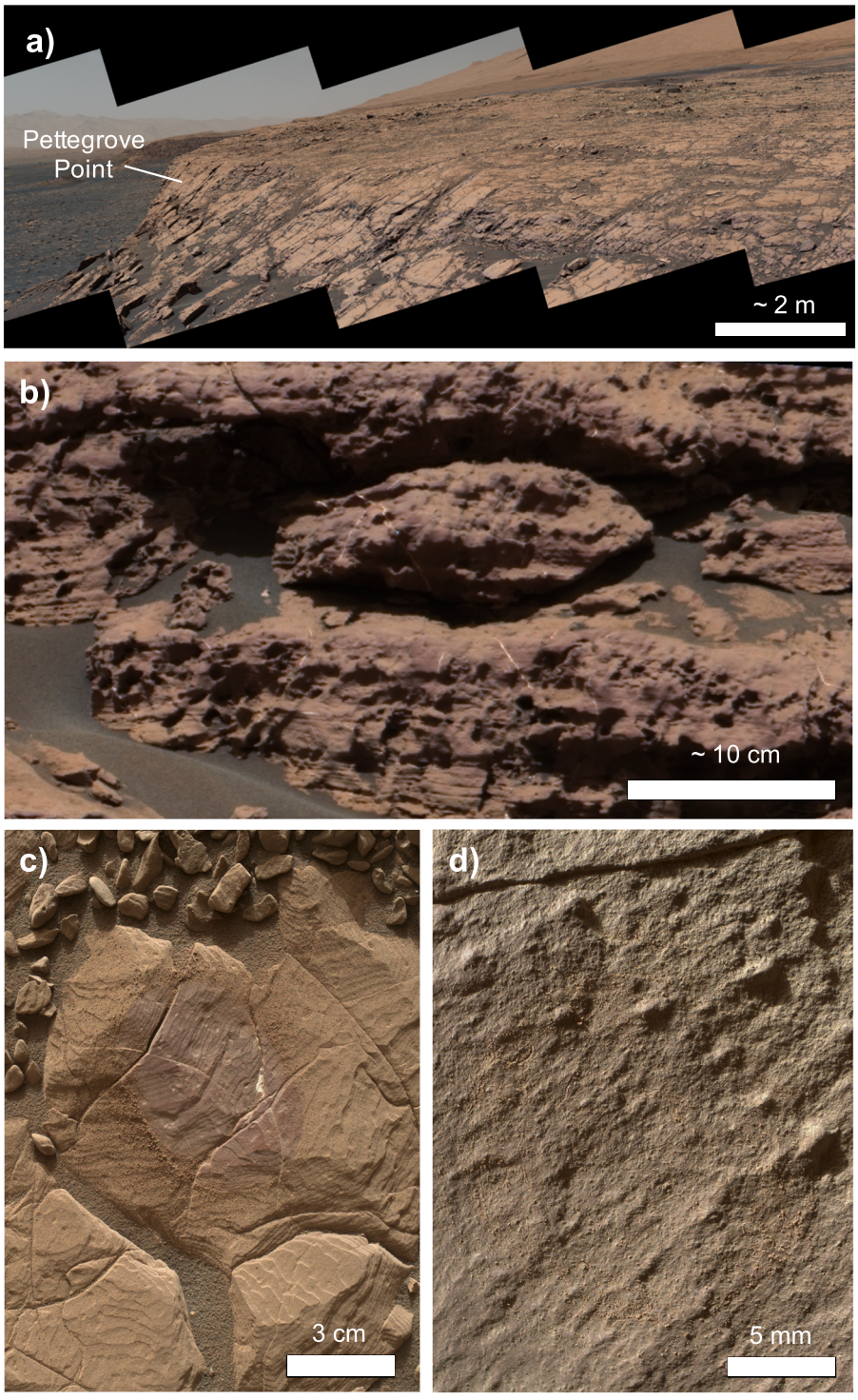

Figure 8. A) Pettegrove Point member observed at the initial ascent of Vera Rubin ridge. Fine, parallel lamination can be traced across the outcrop with no disruption. Mosaic includes the "Pettegrove Point" target for which this member was named. Mastcam mosaic acquired on sol 1,812 by the M34 camera, sequence mcam09356. (b) An outcrop of the Pettegrove Point member showing resistant outcrop with a higher abundance of nodules, and fewer veins than the Blunts Point member. Planar lamination is observed throughout. Mastcam image acquired on sol 1,829 by the M100 camera, sequence mcam09462. (c) Mars Hand Lens Imager (MAHLI) imaging reveals fine-grain sizes and thin parallel lamination. The center of the image reveals the Dust Removal Tool (DRT) target "Mitten Ledge." MAHLI image acquired on sol 1,818 from 25-cm standoff. MAHLI image 1818MH0001900010701460C00. (d) Several targets within the Pettegrove Point member also show evidence for fine sand grains. MAHLI image of "Sherwood Forest" acquired on sol 1,824 from 1-cm standoff. MAHLI image 1826MH0007250000701691R00.

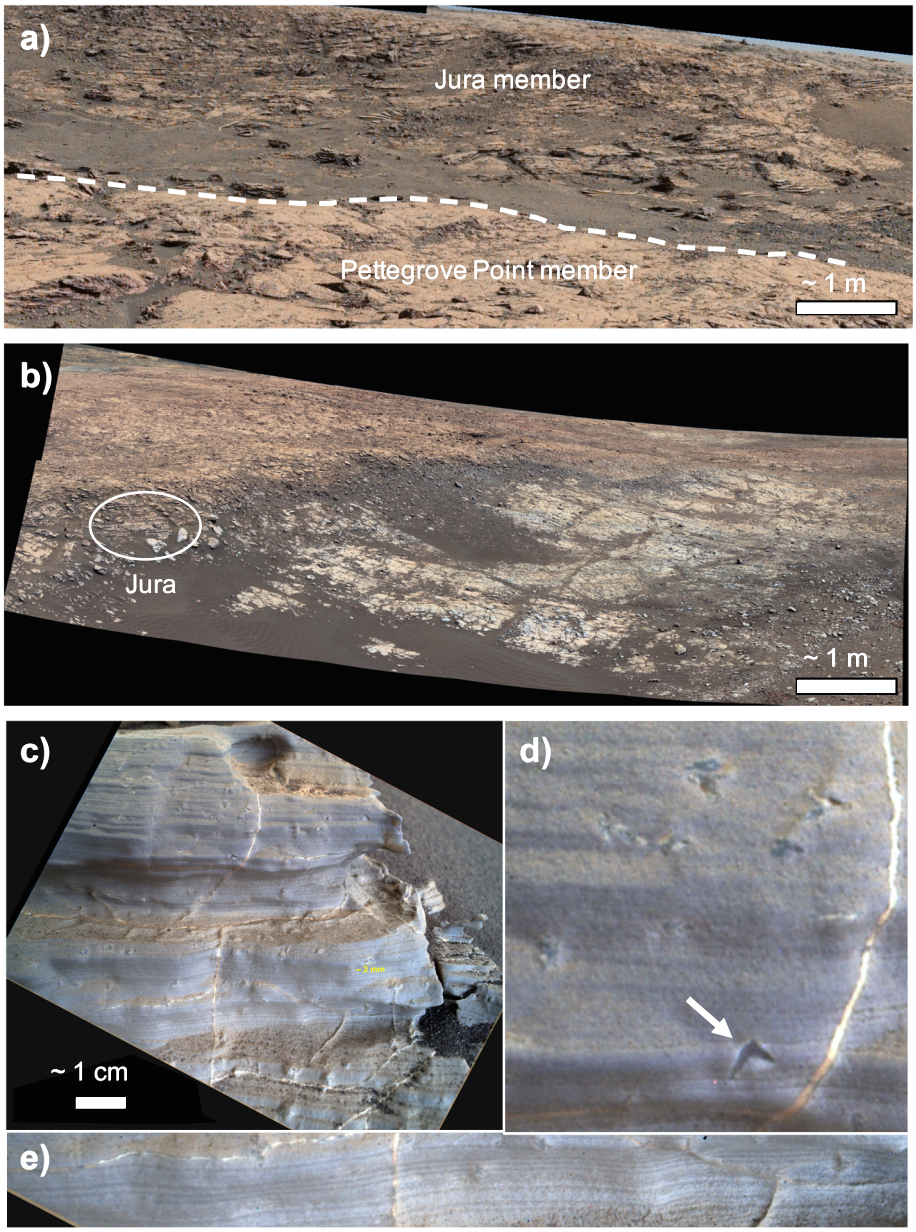

Figure 9. The Jura member observed at the top of Vera Rubin ridge. (a) The white dashed line shows the transition between the Pettegrove Point member and the Jura member. The base of the Jura is defined by a distinct step in topography, which often coincides with inclined beds and the Flodigarry facies. Mastcam mosaic acquired on sol 1,850 by the M34 camera, sequence mcam09680. (b) The red and gray color variations in the vicinity of the "Jura" outcrop, for which this member was named. The white circle includes the "Jura" target and the locations of c–e. Mastcam mosaic acquired on sol 1,909 by the M34 camera, mcam10011. (c) Mars Hand Lens Imager (MAHLI) image of the "Jura" target acquired on sol 1,925 from 10-cm standoff. MAHLI image 1925MH0002910010703326C00. The false color image has been enhanced to highlight stratification. (d) A portion of (c) showing swallowtail crystal molds. (e) A portion of (c) showing fine lamination of variable thickness.

been filled and has since been partly exhumed (Malin & Edgett, 2000), which would lead to substantial compaction of the lower strata of Mount Sharp (Borlina et al., 2015). Sedimentary facies of variable grain size, sorting, cement, and other properties could produce local differences in compaction, which may explain the offset observed at VRR. However, it is equally likely that Gale crater contained a lake or series of lakes (Grotzinger et al., 2015) and that these connected lakes experienced minor gradients in grain size, which manifest as distinct stratigraphic members, and that those lateral variations in facies led to vertical offsets in member boundaries through time, following Walther's law (Walther, 1894).

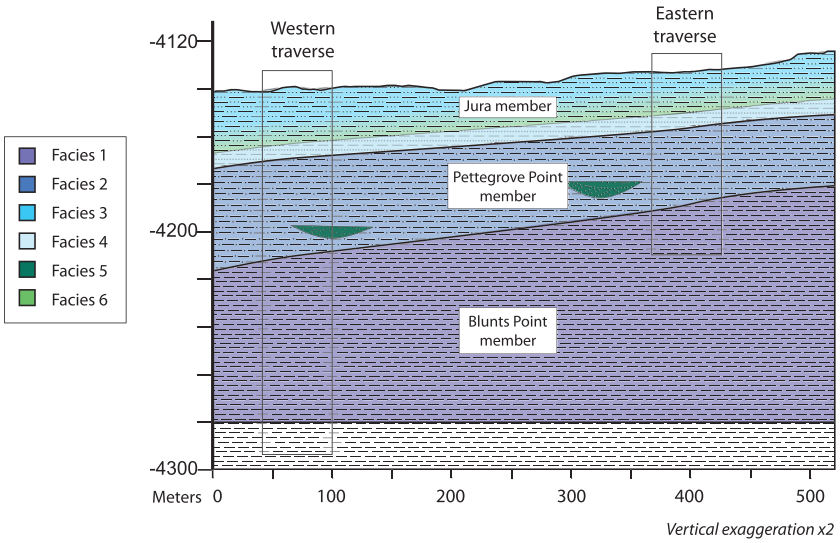

Figure 10. Schematic cross section from west to east across Vera Rubin ridge, illustrating the offset in elevation between stratigraphic members. Colors indicate the distribution of the six facies and their relation to stratigraphic members. Pattern indicates that the dominant lithology is mudstone with an increase in silt and sand content higher in the section. Boxes show the approximate locations of the stratigraphy observed in the western traverse and eastern traverse.

Based on these lateral and vertical variations, the contacts between different stratigraphic members are represented by curved lines on the stratigraphic column (Figure 11) to indicate the observed elevations of these contacts as context for chemostratigraphic studies (Frydenvang et al., 2018; Thompson et al., 2019).

7. Deformation

The primary depositional layering of the strata that comprise VRR are generally interpreted to be horizontal (Stein et al., 2019). At the outcrop scale, individual laminae can be traced for up to several meters, and strike and dip measurements indicate relatively flat orientations, varying just a couple of degrees (Stein et al., 2019). Further constraints on bedding orientation come from stratigraphic correlations, and the observation that Facies 4 (Flodigarry facies), which marks the base of the Jura member, can be identified beyond VRR in the Glen Torridon region (Stein et al., 2019). The elevation at which this facies occurs on VRR and in Glen Torridon, separated by nearly 100 m laterally, requires the strata to be generally horizontal in a north to south direction.

However, there are localized regions in which the strata are clearly not flat-lying, as shown by the large-scale inclined beds of Facies 6. These inclined beds generally mark the base of the Jura member, in association with Facies 4 (Flodigarry facies), and correspond to a break in slope. The observation of domal, concave-down structures with traceable laminae suggests at least partial lithification prior to ductile deformation.

One such structure was observed on VRR between sols 1,848–1,867 and has an antiformal structure. This structure was best documented from the sol 1,864 end-of-drive location, using the M34 camera (Figure 12a). Here, the antiform is highlighted by laminations characteristic of the Murray formation, which dip away from a central crest area, where the laminations have an apparent zero degree dip. From the sol 1,864 end-of-drive location, the structure has a measured vertical height of ~0.8 m, and the face of the outcrop where the fold is observed has a width of ~20 m. The two limbs of the antiform can be observed to dip shallowly away from the crest of the structure, with apparent angle of dip between 10 and 20°, giving the fold an apparent interlimb angle of ~140°—a gentle fold (Figure 12b). Using the methods for estimating dip orientation described by Banham et al. (2018), dip-azimuth measurements were derived and mapped to determine the shape and orientation of the structure (Figure 12c). The western limb of the structure, while partially eroded and covered with windblown sand, was observed to dip with an apparent orientation toward the northwest (~310°). The east limb of the structure, which is better exposed, demonstrates a dip direction toward the southeast (~116°). The axis of this fold is oriented approximately NE-SW (Figure 12c). Whether or not the fold is plunging toward the south cannot be ascertained due to

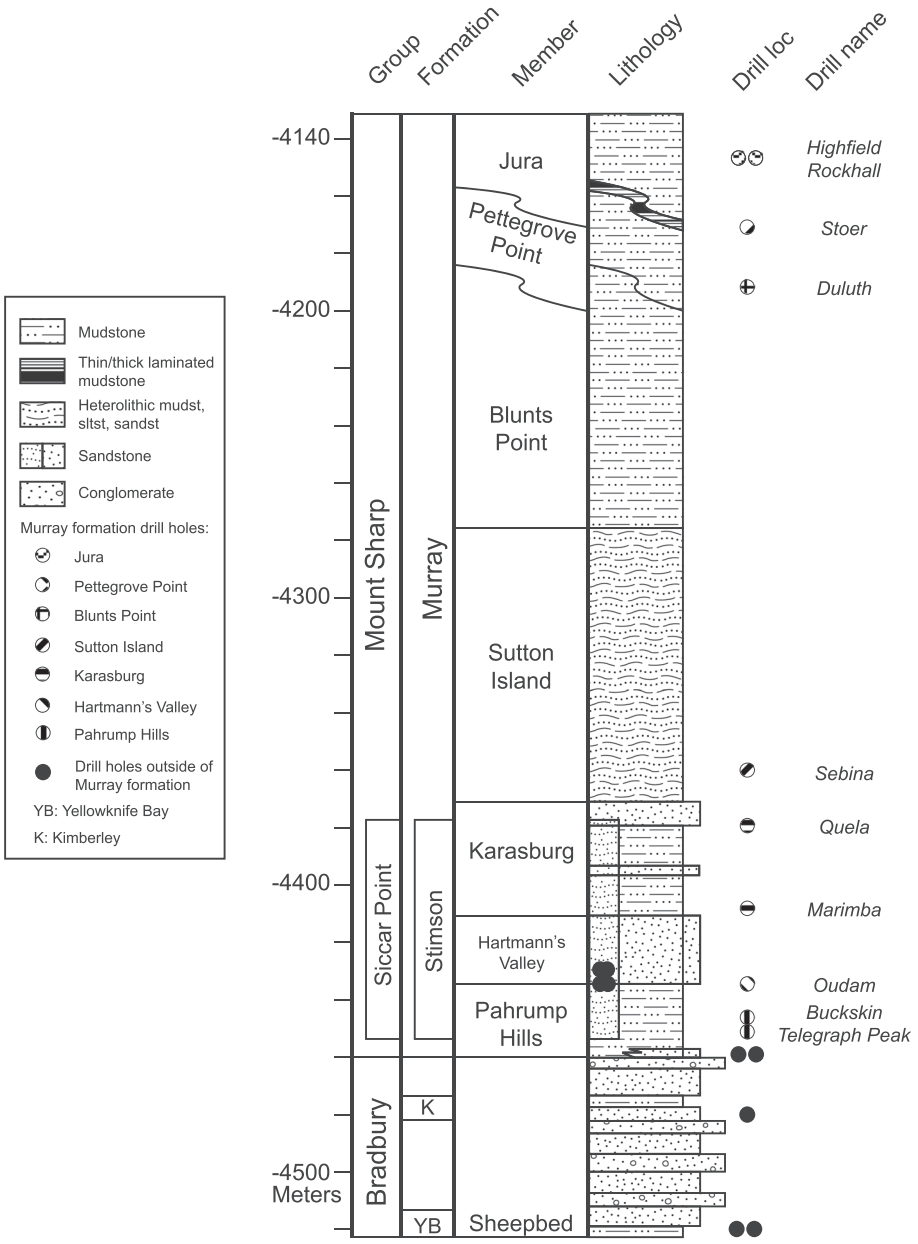

Figure 11. Generalized stratigraphic column extended through Vera Rubin ridge (VRR). Contacts between VRR stratigraphic members are shown as sinuous lines to indicate the observed change in elevations across VRR. Flodigarry marker is represented by white boundary at the base of the Jura member. Drill locations within the Murray formation are marked by distinct symbols to differentiate the targets, as indicated in the legend.

uncertainty associated with the measurement of the fold limbs. When the east limb of the fold is viewed perpendicular to strike from the sol 1,869 end-of-drive location, no preferential apparent dip can be discerned in the Navcam mosaic, suggesting that the fold is not plunging. The antiform structure is approximately 20 m across, and each of the limbs are approximately 10–12 m across. It should be noted that the face observed in Figures 12a and 12b is oblique to the structure, as mapped out in Figure 12c. The antiform structure may record a subaqueous slump that occurred soon after deposition. Water-laden layers of sediment would have accumulated on a slope, which would have resulted in sediment moving down slope under the influence of gravity. The axis and shortening direction of the fold would imply that the slope was dipping in a NW-SE direction. An alternative hypothesis for the antiform is that the fold could have been generated by meteoric impact, although this particular fold is not associated with any visible impact craters.

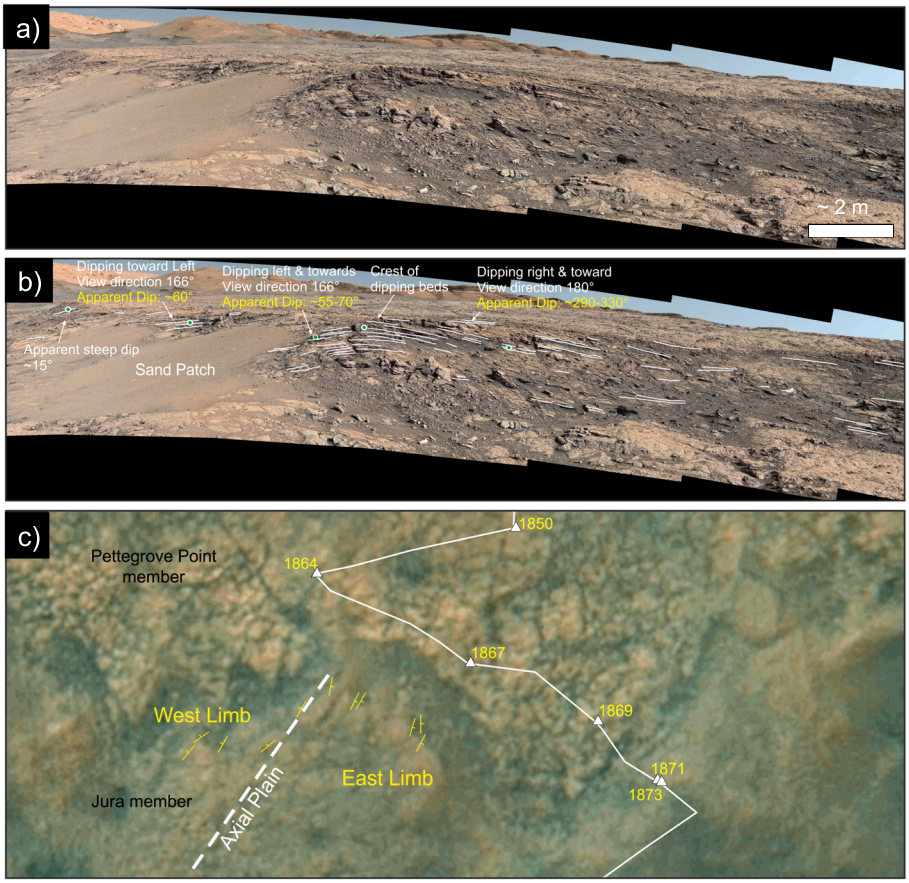

Figure 12. Inclined beds observed during sols 1,848–1,867. (a) Mastcam M34 mosaic acquired on sol 1,864. View is approximately toward the south. (b) Interpreted view of (a). Beds dip away from a central crest. Apparent dip direction reported in yellow. (c) High Resolution Imaging Science Experiment (HiRISE) image showing the antiform structure in plan view. The dashed white line shows the approximate axis of the antiform. The solid white line shows the rover's traverse path. Note that the contact between the fractured Pettegrove Point member to the north and the darker smoother Jura member to the south is also visible in this image. The inclined beds occur at the base of the Jura member.

Another location with inclined beds, informally named "Glen Tilt," is associated with an inferred impact structure. The "Glen Tilt" structure was observed from the sols 1,942 and 1,944 end-of-drive locations. From the sol 1,942 position (Figure 13a), laminated beds can be observed, which form a north-south trending ridge, that demarks the southwest rim of a degraded crater. Within the north section of that ridge, beds are observed to dip shallowly toward the east with an apparent dip of ~10–15°. To the south, where the ridge curves to the east, the overall apparent dip direction appears to change toward the northeast. Locally within the ridge, local dip directions change over relatively short distance. From the sol 1,944 end-of-drive position, a small synform-like fold that is approximately 3 m wide can be observed (Figure 13b). This small fold plunges approximately east, which would have been toward the center of the crater. A similar structure, which is largely occluded by regolith, can be observed in the south edge of the crater rim (Figure 13a). These axial fold structures are common in impact crater structures (Kenkmann et al., 2014), and therefore, it is inferred that the Glen Tilt deformation structures may be related to an impact event that occurred after partial lithification.

8. Diagenesis

VRR is a thick succession of lacustrine deposits that encountered variable diagenetic episodes. Evidence for diagenesis is manifested through notable red and gray color variations that cut across primary stratification (Fraeman et al., 2018; Horgan et al., 2019), millimeter- to centimeter-scale features such as crystal

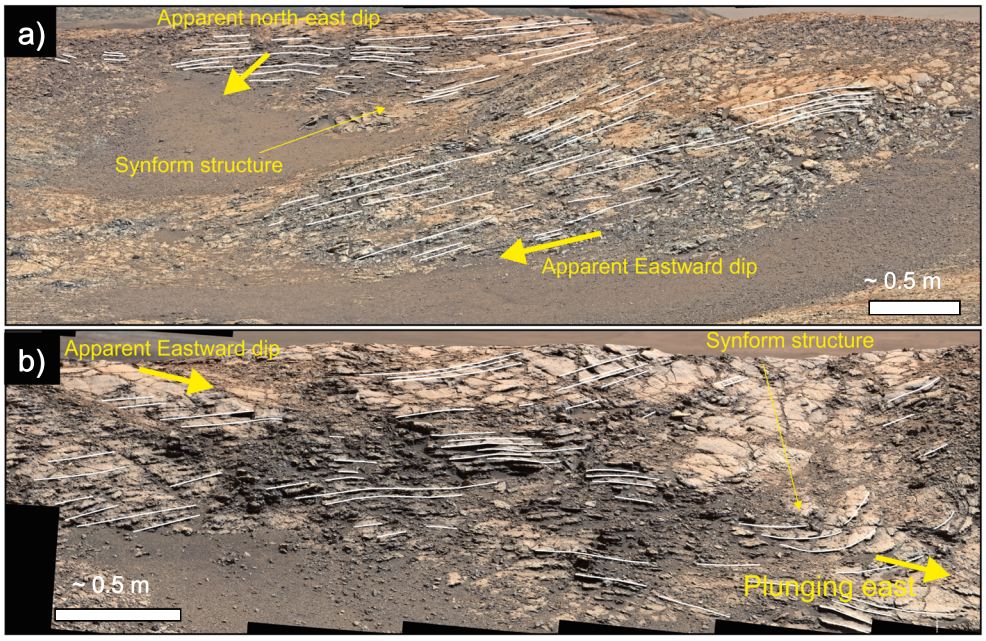

Figure 13. Inclined beds at "Glen Tilt," observed during sols 1,942–1,944. (a) View from the sol 1,942 position, looking toward the southwestern rim of the crater at azimuth 235°. Beds in the lower half of the image dip toward the left, which is approximately to the southeast, while beds in the upper half of the image dip toward the viewer, which is approximately to the northeast. (b) View from the sol 1,944 location, view toward azimuth 285°, showing a small synform structure that appears to be plunging toward the east.

pseudomorphs, nodules, and dark, diagenetic features (Bennett et al., 2018; L'Haridon et al., 2019), and abundant fractures containing calcium sulfate veins of variable orientation (Fedo et al., 2018). Details of the diagenetic history revealed from MAHLI images are summarized by Bennett et al. (2018) and include the following episodes: (1) early diagenesis including lithification of parts of the Jura member and precipitation of crystals, (2) dissolution and replacement of original crystals, (3) precipitation of nodules, and (4) development of various generations of calcium sulfate veins. Further evidence for a complex diagenetic history is the occurrence of the ridge as a discrete topographic feature, thought to result from enhanced crystallization and cementation due to warm fluids (Fraeman et al., 2018; Morris et al., 2019).

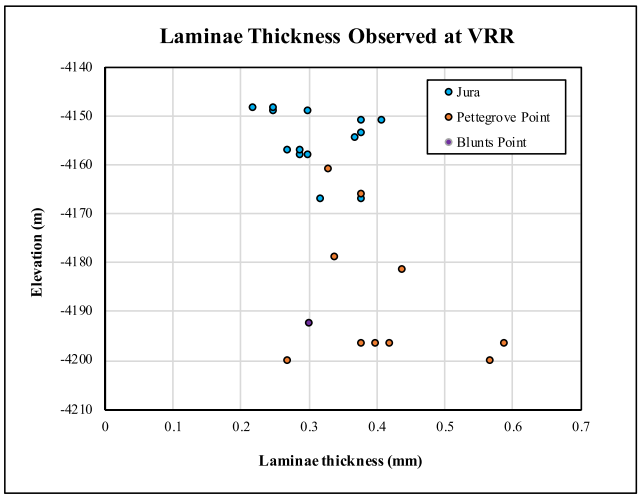

Figure 14. Average laminae thickness for twenty-five targets observed at Vera Rubin ridge. Targets are plotted as a function of elevation. The orange data points correspond to targets within the Pettegrove Point member, the blue data points correspond to the Jura member, and the purple data point represents the "Duluth" target in the Blunts Point member.

9. Implications for the Duration of Habitable Conditions

Exploration of VRR reveals that the stratigraphic section of lacustrine mudstones is continuous for much of the lower Murray and is at least 300+ m thick. From Curiosity's first encounter with the Murray formation at the Pahrump Hills (Grotzinger et al., 2015; Stack et al., 2019) to the top of VRR, Curiosity has gained 314 m in elevation. Rocks exposed on the VRR constitute a significant fraction of the stratigraphic thickness of the Murray formation. The facies observed in the 314 m of the full Murray formation are consistent with lake and lake margin environments (Fedo et al., 2019; Grotzinger et al., 2015; Rivera-Hernández et al., 2020; Stack et al., 2019). Comparison of the average laminae thickness at VRR (ranging from 0.22 to 0.59 mm; Figure 14) to laminae observed at the Pahrump Hills (ranging from 0.2 to 0.55 mm, Grotzinger et al., 2015) suggests comparable sediment input and depositional processes. Previous work has considered the finely laminated mudstone facies of the

Murray formation to be generated by either hyperpycnal or hypopycnal sediment plumes as the delivery mechanism for sediment into the lake basin (Grotzinger et al., 2015; Stack et al., 2019). When the Murray formation was first encountered, Grotzinger et al. (2015) used a 75-m stratigraphic thickness of the Murray formation, combined with laminae thickness and scaled to terrestrial deposition rates (Sadler et al., 1981) to estimate a duration of 10^4 to 10^7 years for accumulation. Stack et al. (2019) considered individual laminae in the 13-m-thick Pahrump Hills section to be event beds and estimated a minimum duration for the Pahrump Hills section on the order of 10^3 years if these events occurred seasonally, and a maximum duration of up to 10^7 years if hyperpycnal flows occurred at more rare intervals.

Here we use new data to confirm lacustrine deposition through VRR and build on previous work to estimate the duration of habitable conditions in Gale crater. Rates of lacustrine sedimentation on Earth typically range from 0.01 to 0.12 cm/year (Robbins & Edgington, 1975) to 0.29 to 9.5 cm/year (Sekar et al., 2010) depending on climatic influences and methods for age and rate determination. Based on the 314-m thickness of the Murray formation and the range of sedimentation rates achieved in terrestrial settings, the Murray formation would have required a minimum of 10^5 to 10^6 years to form. However, the Murray formation also likely endured substantial compaction and erosion. Based on terrestrial compaction curves for shales (Baldwin & Butler, 1985), and assuming that the strata were likely buried by more than 2 km of sediment (Grotzinger et al., 2015; Malin & Edgett, 2000), we estimate that the stratigraphic thickness of the Murray formation represents only part of its original thickness (77% according to the Dickinson curve) and therefore suggest that aqueous environments existed in Gale crater in excess of 10^6 years. While previous studies supplied similar estimates for the duration of a lake or series of lakes in Gale crater, exploration of VRR significantly expands the duration of habitable conditions that can be confirmed through ground truth of lacustrine environments.

Curiosity has a lot more stratigraphic section to climb and explore within Gale crater, and tens of meters more that may be attributed to the Murray formation based on similar outcrop erosional expressions as seen in HiRISE images. The sedimentary facies and stratigraphic members identified here serve as a guide for future exploration within the Glen Torridon region (Bennett et al., 2019) and beyond.

10. Conclusions

Curiosity's exploration of VRR is, to date, the longest duration and most thorough investigation of lacustrine strata on Mars. The VRR campaign provided a rare opportunity in the MSL mission to perform two distinct transects through a stratigraphic section. Through identification of sedimentary facies and stratigraphic correlations, the following conclusions can be drawn:

1. The members within the VRR and the Blunts Point member are composed of six sedimentary facies. These facies are consistent with deposition in a dominantly low-energy lacustrine environment. A few outcrops of low-angle stratification suggest possible influences by subaqueous currents. Inclined beds suggest minor deformation and are inferred to be a result of small slope failures and slumping. However, the vast majority of the strata at VRR consist of fine-grained, parallel-stratified facies with few disruptions and no desiccation cracks or other evidence of subaerial exposure, which suggests relatively stable water levels throughout its deposition.
2. The facies described here are part of the Murray formation and can be subdivided into three stratigraphic members: Blunts Point member, Pettegrove Point member, and the Jura member, with the latter two members forming the topographic ridge. A distinct facies at the base of the Jura member may serve as a marker for recognizing this transition.
3. Grain size and laminae thicknesses are consistent with previous observations within the Murray formation. Observations from MAHLI and ChemCam LIBS data indicate that grain sizes are typically mud to very fine sand. A slight coarsening upward sequence is observed as the Jura member has a higher proportion of targets with observable coarser grains than the underlying strata. Laminae thicknesses across VRR range from 0.22 to 0.59 mm, which is similar to previously reported laminae thicknesses in lower strata of the Murray formation (Grotzinger et al., 2015; Stack et al., 2019).
4. Stratigraphic correlation across two distinct transects indicates that the boundaries between stratigraphic members crosscut elevation. The elevation difference suggests either the result of differential compaction or that the contacts between these members record lateral variations in facies.

5. No significant gaps in the stratigraphic record are observed. The strata exposed at VRR significantly expand the duration of habitable conditions observed in Gale crater and suggest that aqueous environments existed in Gale crater in excess of 10^6 years.
6. The sedimentary facies and stratigraphic members identified at VRR serve as a framework for interpreting strata within the Glen Torridon region and beyond.

Acknowledgments
The authors gratefully acknowledge support from the NASA MSL mission and the efforts of the MSL engineering and science operations teams. A portion of this research was carried out at the Jet Propulsion Laboratory, California Institute of Technology, under a contract with the National Aeronautics and Space Administration. A portion of this work was supported by the Simons Collaboration for the the Origin of Life. All of the Mastcam, Navcam, Hazcam, MARDI, and MAHLI images used in this manuscript are freely available through the Planetary Data System Cartography and Imaging Sciences node (https://pds-imaging.jpl.nasa.gov/volumes/msl.html). All of the ChemCam RMI images used in this manuscript are freely available through the Planetary Data System Geosciences node (https://pds-geosciences.wustl.edu/missions/msl/chemcam.htm). Data used to estimate grain size using the Gini index can be accessed via Zenodo: https://doi.org/10.5281/zenodo.3605603 (sols 766–1,804) and https://doi.org/10.5281/zenodo.3672073 (1808-2298). Data used to estimate laminae thickness can be accessed via Zenodo: http://doi.org/10.5281/zenodo.3672078.

References

Baldwin, B., & Butler, C. O. (1985). Compaction curves. *AAPG Bulletin*, *69*(4), 622–626. https://doi.org/10.1306/AD462547-16F7-11D7-8645000102C1865D

Banham, S. G., Gupta, S., Rubin, D. M., Watkins, J. A., Sumner, D. Y., Edgett, K. S., et al. (2018). Ancient Martian aeolian processes and palaeomorphology reconstructed from the Stimson formation on the lower slope of Aeolis Mons, Gale crater, Mars. *Sedimentology*, *65*(4), 993–1042. https://doi.org/10.1111/sed.12469

Bennett, K. A., Edgett, K., Fey, D., Edgar, L. A., Fraeman, A., McBride, M., & Edwards, C. (2018). Fine-scale textural observations at Vera Rubin Ridge, Gale crater, from the Mars Hand Lens Imager (MAHLI). *LPI* (2083), 1769.

Bennett, K. A., Fox, V. K., Bryk, A. B., Fedo, C., Vasavada, A. R., Dehouck, E., et al. (2019). Results from the Curiosity rover's traverse through the clay-bearing Glen Torridon Region in Gale crater. Presented at the AGU Fall Meeting 2019, AGU. Retrieved from. https://agu.confex.com/agu/fm19/meetingapp.cgi/Paper/506844

Borlina, C. S., Ehlmann, B. L., & Kite, E. S. (2015). Modeling the thermal and physical evolution of Mount Sharp's sedimentary rocks, Gale crater, Mars: Implications for diagenesis on the MSL Curiosity rover traverse. *Journal of Geophysical Research, Planets*, *120*(8), 1396–1414. https://doi.org/10.1002/2015JE004799

Edgar, L. A., Gupta, S., Rubin, D. M., Lewis, K. W., Kocurek, G. A., Anderson, R. B., et al. (2017). Shaler: in situ analysis of a fluvial sedimentary deposit on Mars. *Sedimentology*, *65*(1), 96–122. https://doi.org/10.1111/sed.12370

Edgett, K. S., Yingst, R. A., Ravine, M. A., Caplinger, M. A., Maki, J. N., Ghaemi, F. T., et al. (2012). Curiosity's Mars Hand Lens Imager (MAHLI) investigation. *Space Science Reviews*, *170*(1-4), 259–317. https://doi.org/10.1007/s11214-012-9910-4

Farmer, J. D., & DesMarais, J. D. (1999). Exploring for a record of ancient Martian life. *Journal of Geophysical Research*, *104*(E11), 26,977–26,995. https://doi.org/10.1029/1998JE000540

Fedo, C., Grotzinger, J. P., Gupta, S., Banham, S., Bennett, K., Edgar, L. A., et al. (2019). Evidence for persistent, water-rich lacustrine deposition preserved in the Murray formation, Gale crater: A depositional system suitable for sustained habitability. Presented at the Ninth International Conference on Mars. Retrieved from. https://www.hou.usra.edu/meetings/ninthmars2019/pdf/6308.pdf

Fedo, C. M., Grotzinger, J. P., Schieber, J., Gupta, S., House, C. H., Edgett, K. S., et al. (2018). Things are not always as they seem: Detangling intersecting planar and curvi-planar veins and fractures from primary bedding in the Vera Rubin ridge member, Murray formation, Mars. *Geological Society of America Abstracts with Programs*, *50*(3). https://doi.org/10.1130/abs/2018SE-312748

Flood, R. D., & Giosan, L. (2002). Migration history of a fine-grained abyssal sediment wave on the Bahama Outer Ridge. *Marine Geology*, *192*(1), 259–273. https://doi.org/10.1016/S0025-3227(02)00558-3

Fraeman, A., Sun, V. Z., Edgar, L. A., Fedo, C., Fox, V. K., Grotzinger, J. P., et al. (2018). Curiosity at Vera Rubin Ridge: Major findings and implications for habitability. *AGUFM*, *2018*, P41A–02–02.

Fraeman, A. A., Arvidson, R. E., Catalano, J. G., Grotzinger, J. P., Morris, R. V., Murchie, S. L., et al. (2013). A hematite-bearing layer in Gale crater, Mars: Mapping and implications for past aqueous conditions. *Geology*, *41*(10), 1103–1106. https://doi.org/10.1130/G34613.1

Fraeman, A. A., Ehlmann, B. L., Arvidson, R. E., Edwards, C. S., Grotzinger, J. P., Milliken, R. E., et al. (2016). The stratigraphy and evolution of lower Mount Sharp from spectral, morphological, and thermophysical orbital data sets. *Journal of Geophysical Research, Planets*, *121*(9), 1713–1736. https://doi.org/10.1002/2016JE005095

Frydenvang, J., Mangold, N., Wiens, R. C., Fraeman, A., Fedo, C., l'Haridon, J., et al. (2018). Geochemical evidence from the ChemCam instrument highlighting the role of diagenesis at Vera Rubin Ridge in Gale crater, Mars. *AGUFM*, *2018*, P41A–06–06.

Golombek, M., Grant, J., Kipp, D., Vasavada, A., Kirk, R., Fergason, R., et al. (2012). Selection of the Mars Science Laboratory Landing Site. *Space Science Reviews*, *170*(1-4), 641–737. https://doi.org/10.1007/s11214-012-9916-y

Grotzinger, J. P., Crisp, J., Vasavada, A. R., Anderson, R. C., Baker, C. J., Barry, R., et al. (2012). Mars Science Laboratory mission and science investigation. *Space Science Reviews*, *170*(1-4), 5–56. https://doi.org/10.1007/s11214-012-9892-2

Grotzinger, J. P., Gupta, S., Malin, M. C., Rubin, D. M., Schieber, J., Siebach, K., et al. (2015). Deposition, exhumation, and paleoclimate of an ancient lake deposit, Gale crater, Mars. *Science*, *350*(6257), aac7575. https://doi.org/10.1126/science.aac7575

Grotzinger, J. P., Sumner, D. Y., Kah, L. C., Stack, K., Gupta, S., Edgar, L., et al. (2014). A habitable fluvio-lacustrine environment at Yellowknife Bay, Gale crater, Mars. *Science*, *343*(6169), 1242777. https://doi.org/10.1126/science.1242777

Gwizd, S., Fedo, C., Grotzinger, J., Edgett, K., Gupta, S., Stack, K. M., et al. (2019). Toward a greater understanding of cross-stratified facies in the Hartmann's Valley member of the Murray formation, Gale crater, Mars. In the Ninth International Conference on Mars, Abstract #6183.

Gwizd, S., Fedo, C., Grotzinger, J., Edgett, K., Rivera-Hernández, F., & Stein, N. (2018). Depositional History of the Hartmann's Valley Member, Murray Formation, Gale crater, Mars. In the 49th Lunar and Planetary Science Conference, Abstract #2150.

Hays, L. E., Graham, H. V., Des Marais, D. J., Hausrath, E. M., Horgan, B., McCollom, T. M., et al. (2017). Biosignature preservation and detection in Mars analog environments. *Astrobiology*, *17*(4), 363–400. https://doi.org/10.1089/ast.2016.1627

Horgan, B., Fraeman, A., Johnson, J. R., Thompson, L., Jacob, S., Bell, J. F., & Grotzinger, J. (2019). Redox conditions during diagenesis in the Vera Rubin Ridge, Gale crater, Mars, from Mastcam Multispectral Images. *LPI* (2132), 1424.

Kenkmann, T., Poelchau, M. H., & Wulf, G. (2014). Structural geology of impact craters. *Journal of Structural Geology*, *62*, 156–182. https://doi.org/10.1016/j.jsg.2014.01.015

Le Deit, L., Hauber, E., Fueten, F., Mangold, N., Pondrelli, M., Rossi, A., & Jaumann, R. (2012). Model age of Gale crater and origin of its layered deposits. *LPICo*, *1680*, 7045.

Le Mouélic, S., Gasnault, O., Herkenhoff, K. E., Bridges, N. T., Langevin, Y., Mangold, N., et al. (2015). The ChemCam remote micro-imager at Gale crater: Review of the first year of operations on Mars. *Icarus*, *249*, 93–107. https://doi.org/10.1016/j.icarus.2014.05.030

L'Haridon, J., Mangold, N., Wiens, R. C., Cousin, A., David, G., Johnson, J. R., et al. (2019). Iron-rich diagenetic features analysed in the Murray formation at Gale crater, Mars, Using Chemcam Onboard the Curiosity Rover. *LPICo*, *2089*, 6079.

Maki, J., Thiessen, D., Pourangi, A., Kobzeff, P., Litwin, T., Scherr, L., et al. (2012). The Mars Science Laboratory engineering cameras. *Space Science Reviews*, *170*(1-4), 77–93. https://doi.org/10.1007/s11214-012-9882-4

Malin, M. C., & Edgett, K. S. (2000). Sedimentary rocks of early Mars. *Science*, *290*(5498), 1927–1937. https://doi.org/10.1126/science.290.5498.1927

Malin, M. C., Ravine, M. A., Caplinger, M. A., Ghaemi, F. T., Schaffner, J. A., Maki, J. N., et al. (2017). The Mars Science Laboratory (MSL) Mast cameras and Descent imager: Investigation and instrument descriptions. *Earth and Space Science*, *4*(8), 506–539. https://doi.org/10.1002/2016EA000252

Maurice, S., Wiens, R. C., Saccoccio, M., Barraclough, B., Gasnault, O., Forni, O., et al. (2012). The ChemCam Instrument Suite on the Mars Science Laboratory (MSL) Rover: Science objectives and Mast unit description. *Space Science Reviews*, *170*(1-4), 95–166. https://doi.org/10.1007/s11214-012-9912-2

Meyers, P. A., & Ishiwatari, R. (1995). Organic Matter Accumulation Records in Lake Sediments. In A. Lerman, D. M. Imboden, & J. R. Gat (Eds.), *Physics and Chemistry of Lakes*, (pp. 279–328). Berlin, Heidelberg: Springer Berlin Heidelberg. Retrieved from. https://doi.org/10.1007/978-3-642-85132-2_10

Milliken, R. E., Grotzinger, J. P., & Thomson, B. J. (2010). Paleoclimate of Mars as captured by the stratigraphic record in Gale Crater. *Geophysical Research Letters*, *37*(4). https://doi.org/10.1029/2009GL041870

Minitti, M. E., Malin, M. C., Van Beek, J. K., Caplinger, M., Maki, J. N., Ravine, M., et al. (2019). Distribution of primary and secondary features in the Pahrump Hills outcrop (Gale crater, Mars) as seen in a Mars Descent Imager (MARDI) "sidewalk" mosaic. *Icarus*, *328*, 194–209. https://doi.org/10.1016/j.icarus.2019.03.005

Morris, R. V., Bristow, T. F., Rampe, E. B., Yen, A. S., Vaniman, D. T., Tu, V., et al. (2019). Mineralogy and formation processes for the Vera Rubin ridge at Gale crater, Mars from CheMin XRD Analyses. *LPI* (2132), 1127.

Rampe, E. B., Ming, D. W., Blake, D. F., Bristow, T. F., Chipera, S. J., Grotzinger, J. P., et al. (2017). Mineralogy of an ancient lacustrine mudstone succession from the Murray formation, Gale crater, Mars. *Earth and Planetary Science Letters*, *471*, 172–185. https://doi.org/10.1016/j.epsl.2017.04.021

Rice, M. S., Gupta, S., Treiman, A. H., Stack, K. M., Calef, F., Edgar, L. A., et al. (2017). Geologic overview of the Mars Science Laboratory rover mission at the Kimberley, Gale crater, Mars. *Journal of Geophysical Research, Planets*, *122*(1), 2–20. https://doi.org/10.1002/2016JE005200

Rivera-Hernández, F., Sumner, D. Y., Mangold, N., Banham, S. G., Edgett, K. S., Fedo, C. M., et al. (2020). Grain size variations in the Murray formation: Stratigraphic evidence for changing depositional environments in Gale crater, Mars. *Journal of Geophysical Research, Planets*, *125*. https://doi.org/10.1029/2019JE006230

Rivera-Hernández, F., Sumner, D. Y., Mangold, N., Stack, K. M., Forni, O., Newsom, H., et al. (2019). Using ChemCam LIBS data to constrain grain size in rocks on Mars: Proof of concept and application to rocks at Yellowknife Bay and Pahrump Hills, Gale crater. *Icarus*, *321*, 82–98. https://doi.org/10.1016/j.icarus.2018.10.023

Robbins, J. A., & Edgington, D. N. (1975). Determination of recent sedimentation rates in Lake Michigan using Pb-210 and Cs-137. *Geochimica et Cosmochimica Acta*, *39*(3), 285–304. https://doi.org/10.1016/0016-7037(75)90198-2

Sadler, P. M. (1981). Sediment accumulation rates and the completeness of stratigraphic sections. *The Journal of Geology*, *89*(5), 569–584. https://doi.org/10.1086/628623

Sekar, B., Bera, S., Bhattacharyya, A., & Nautiyal, C. (2010). Analyses of sedimentation rate and organic matter content in lacustrine sediment profiles from diversified geographical regions of Indian sub-continent and their climatic implications. *International Journal of Earth Sciences and Engineering*, *3*, 775–783.

Stack, K. M., Grotzinger, J. P., Lamb, M. P., Gupta, S., Rubin, D. M., Kah, L. C., et al. (2019). Evidence for plunging river plume deposits in the Pahrump Hills member of the Murray formation, Gale crater, Mars. *Sedimentology*, *66*(5), 1768–1802. https://doi.org/10.1111/sed.12558

Stein, N., Grotzinger, J. P., Quinn, D. P., Fedo, C., Stack, K., Edgar, L. A., Fraeman, A. A., & Ehlmann, B. L. (2019). Bedding orientations of the Vera Rubin Ridge, Gale crater, Mars and implications for regional stratigraphy. Presented at the AGU Fall Meeting 2019, AGU. Retrieved from https://agu.confex.com/agu/fm19/meetingapp.cgi/Paper/567357

Stein, N., Grotzinger, J. P., Schieber, J., Mangold, N., Hallet, B., Newsom, H., et al. (2018). Desiccation cracks provide evidence of lake drying on Mars, Sutton Island member, Murray formation, Gale crater. *Geology*, *46*(6), 515–518. https://doi.org/10.1130/G40005.1

Summons, R. E., Amend, J. P., Bish, D., Buick, R., Cody, G. D., Des Marais, D. J., et al. (2011). Preservation of Martian organic and environmental records: Final report of the Mars Biosignature Working Group. *Astrobiology*, *11*(2), 157–181. https://doi.org/10.1089/ast.2010.0506

Taylor, K. H., & Purkis, S. J. (2012). Evidence for the southward migration of mud banks in Florida Bay. *Marine Geology*, *311-314*, 52–56. https://doi.org/10.1016/j.margeo.2012.04.007

Thompson, L. M., Fraeman, A. A., Berger, J. A., Rampe, E. B., Boyd, N. I., Gellert, R., et al. (2019). Compositional characteristics and trends within the Vera Rubin Ridge, Gale crater, Mars as determined by APXS: Sedimentary, diagenetic, and alteration history. *LPI* (2132), 3269.

Thomson, B. J., Bridges, N. T., Milliken, R., Baldridge, A., Hook, S. J., Crowley, J. K., et al. (2011). Constraints on the origin and evolution of the layered mound in Gale crater, Mars using Mars Reconnaissance Orbiter data. *Icarus*, *214*(2), 413–432. https://doi.org/10.1016/j.icarus.2011.05.002

Walther, J. (1894). Einleitung in die geologie als historische wissenschaft: Beobachtungen über die bildung der gesteine und ihrer organischen einschlüsse. G. Fischer.

Wiens, R., Maurice, S., Barraclough, B., Saccoccio, M., Barkley, W. C., Bell, J. F. III, et al. (2012). The ChemCam Instrument Suite on the Mars Science Laboratory (MSL) Rover: Body Unit and Combined System Tests. *Space Science Reviews*, *170*(1-4), 167–227. https://doi.org/10.1007/s11214-012-9902-4

Williams, R. M. E., Grotzinger, J. P., Dietrich, W. E., Gupta, S., Sumner, D. Y., Wiens, R. C., et al. (2013). Martian fluvial conglomerates at Gale crater. *Science*, *340*(6136), 1068–1072. https://doi.org/10.1126/science.1237317

Yingst, R. A., Edgett, K. S., Kennedy, M. R., Krezoski, G. M., McBride, M. J., Minitti, M. E., et al. (2016). MAHLI on Mars: Lessons learned operating a geoscience camera on a landed payload robotic arm. *Geoscientific Instrumentation, Methods and Data Systems*, *5*, 205–217. https://doi.org/10.5194/gi-5-205-2016